Development and plasticity of meningeal lymphatic vessels

Salli Antila,[1] Sinem Karaman,[1] Harri Nurmi,[1] Mikko Airavaara,[2] Merja H. Voutilainen,[2] Thomas Mathivet,[3] Dmitri Chilov,[1] Zhilin Li,[1] Tapani Koppinen,[1] Jun-Hee Park,[4] Shentong Fang,[1] Aleksanteri Aspelund,[1] Mart Saarma,[2] Anne Eichmann,[3,5,6] Jean-Léon Thomas,[4,7] and Kari Alitalo[1]

[1]Wihuri Research Institute and Translational Cancer Biology Program, Biomedicum Helsinki, University of Helsinki, Helsinki, Finland
[2]Program in Developmental Biology, Institute of Biotechnology, HiLIFE Unit, University of Helsinki, Helsinki, Finland
[3]Institut National de la Santé et de la Recherche Médicale U970, Paris Cardiovascular Research Center, Paris, France
[4]Department of Neurology, [5]Cardiovascular Research Center, Department of Internal Medicine, and [6]Department of Cellular and Molecular Physiology, Yale University School of Medicine, New Haven, CT
[7]Sorbonne Universités, UPMC Université Paris 06, Institut National de la Santé et de la Recherche Médicale U1127, Centre National de la Recherche Scientifique, AP-HP, Institut du Cerveau et de la Moelle Epinière, Hôpital Pitié-Salpêtrière, Paris, France

The recent discovery of meningeal lymphatic vessels (LVs) has raised interest in their possible involvement in neuropathological processes, yet little is known about their development or maintenance. We show here that meningeal LVs develop postnatally, appearing first around the foramina in the basal parts of the skull and spinal canal, sprouting along the blood vessels and cranial and spinal nerves to various parts of the meninges surrounding the central nervous system (CNS). VEGF-C, expressed mainly in vascular smooth muscle cells, and VEGFR3 in lymphatic endothelial cells were essential for their development, whereas VEGF-D deletion had no effect. Surprisingly, in adult mice, the LVs showed regression after VEGF-C or VEGFR3 deletion, administration of the tyrosine kinase inhibitor sunitinib, or expression of VEGF-C/D trap, which also compromised the lymphatic drainage function. Conversely, an excess of VEGF-C induced meningeal lymphangiogenesis. The plasticity and regenerative potential of meningeal LVs should allow manipulation of cerebrospinal fluid drainage and neuropathological processes in the CNS.

The Journal of Experimental Medicine

INTRODUCTION

Nearly all mammalian tissues are vascularized by blood vessels (BVs) and lymphatic vessels (LVs). In peripheral organs, lymphatic drainage contributes to interstitial fluid (ISF) homeostasis and immune surveillance by draining waste products, macromolecules and immune cells via LNs to systemic blood circulation (Alitalo, 2011; Koltowska et al., 2013). However, although isolated LVs inside the skull and flow of tracers from brain and cerebrospinal fluid (CSF) space to the draining cervical LNs were detected by several groups (His, 1865; Schwalbe, 1869; Földi et al., 1966; Cserr and Knopf, 1992), perivascular and perineural spaces were considered to provide the pathway into extracranial LVs (Tarasoff-Conway et al., 2015), and the concept of a lymphatic vascular system in the eye and central nervous system (CNS) was lacking until recently (Aspelund et al., 2014, 2015; Park et al., 2014; Louveau et al., 2015).

CNS contains unique ISF–CSF exchange and drainage systems for fluid, solutes, and cells (Louveau et al., 2017; Sun et al., 2017). ISF water and small solute exchange through the capillary walls between the BVs and the brain is limited by the blood–brain barrier (BBB). CSF produced in the epithelial cells of the choroid plexus has a similar composition as cerebral ISF, which is dynamically exchanged with CSF and cleared from brain via a perivascular drainage ("glymphatic") system into subarachnoid space (SAS), a reservoir located between the pia mater and arachnoid membrane (Pollay, 2010; Iliff et al., 2012; Jessen et al., 2015). The discovery of meningeal LVs in the dura mater provides an additional exit pathway from the CNS into systemic circulation (Aspelund et al., 2015; Louveau et al., 2015). Given the potential importance of meningeal LVs in the drainage of macromolecules and cells from the CNS and in the etiology and pathogenesis of neurodegenerative, cerebrovascular, and neuroinflammatory diseases, including Alzheimer's disease, stroke, and multiple sclerosis, better knowledge of their development and function is needed.

In mice, LV development begins between embryonic days 9.5 (E9.5) and E10, when groups of venous endothelial cells (ECs) in the common cardinal vein become committed to the lymphatic fate by starting to express the homeobox transcription factor PROX1 (Wigle and Oliver, 1999; Escobedo and Oliver, 2016). After E10, paracrine VEGF-C in-

Correspondence to Kari Alitalo: kari.alitalo@helsinki.fi

Abbreviations used: AAV, adeno-associated viral vector; αSMA, α smooth muscle actin; BBB, blood–brain barrier; BV, blood vessel; CM, cisterna magna; CN, cranial nerve; CNS, central nervous system; COS, confluence of sinuses; CSF, cerebrospinal fluid; dcLN, deep cervical LN; EB, Evans blue; EC, endothelial cell; EdU, 5-ethynyl-2-dioxyuridine; FM, foramen magnum; i.c.m., intracisternal(ly); i.c.v., intracerebroventricular(ly); i.g., intragastric(ally); ISF, interstitial fluid; JV, jugular vein; LEC, lymphatic EC; LV, lymphatic vessel; MMA, middle meningeal artery; PFA, paraformaldehyde; PPA, pterygopalatine artery; RRV, rostral rhinal vein; RT, room temperature; SAS, subarachnoid space; SMC, smooth muscle cell; SS, sigmoid sinus; SSS, superior sagittal sinus; TS, transverse sinus.

The Rockefeller University Press
J. Exp. Med. 2017 Vol. 214 No. 12 3645–3667
https://doi.org/10.1084/jem.20170391

duces the sprouting of VEGFR3-positive lymphatic EC (LEC) progenitors out from the common cardinal vein to form the first lymphatic plexus (Karkkainen et al., 2004; Hägerling et al., 2013). The subsequent expansion of the lymphatic vascular tree occurs mostly by sprouting from pre-existing LVs, a process known as lymphangiogenesis (Vaahtomeri et al., 2017). In addition, cells of unknown origin in the developing heart, skin, and intestine have been shown to form new LVs (Klotz et al., 2015; Martinez-Corral et al., 2015; Stanczuk et al., 2015). The mature lymphatic vasculature consists of absorptive initial LVs and lymph-transporting precollector and collector vessels (Secker and Harvey, 2015; Kazenwadel and Harvey, 2016). However, how and when the meningeal LVs develop and whether they undergo dynamic changes during aging are unknown. Here, we have explored the development and plasticity of these vessels using a variety of genetic models and modulators of lymphangiogenic signal transduction.

RESULTS

The meningeal lymphatic network develops postnatally

Meningeal LV development was analyzed in *Prox1-eGFP* reporter mice, which express enhanced GFP in lymphatic endothelium (Choi et al., 2011). The LEC identity of the eGFP$^+$ cells was confirmed by whole-mount immunofluorescence staining for LV endothelial hyaluronan receptor 1 (LYVE1; Johnson et al., 2017). Analysis of whole-mount preparations of the meningeal layer attached to the skull at various time points after birth indicated that meningeal LV development occurs in a characteristic manner alongside veins, arteries, and cranial and spinal nerves during the first postnatal weeks. The overall development is schematically summarized in Fig. 1 (A and B), Fig. 2 A, and Fig. S1 A. The developing meningeal LVs appeared first around the foramina that form the entry and exit sites for BVs and nerves, forming an extensive network with numerous sprouts until 3–4 wk of age, after which they appeared to stabilize. Although the development always occurred in the same order, variation in the developmental kinetics and patterns of lymphatic plexuses varied somewhat, even within litters. The images shown illustrate representative developmental patterns at specific time points; the essential anatomical structures are named according to (Ruberte et al., 2017).

The first meningeal LVs were observed just before birth at the base of the skull, around the oval opening for the spinal cord called foramen magnum (FM), and around the pterygopalatine artery (PPA), a branch of the internal carotid artery in mice. After birth, LVs flanking the FM, located next to BVs, extended toward each other to join in the ventral midline at ∼P12 (Fig. 1 C). Valves were occasionally observed in these LVs already at P0, and numerous valves were present in the LV network at P20 (Fig. 1, C and D, arrowheads). Around the PPA, a few rudimentary vessels were visible at birth. After P4, these extended along the middle meningeal artery (MMA), forming valves and reaching the parietal bone area by P16, continuing further growth toward the sagittal suture of the skull (Fig. 1, E and F). Although all meningeal LVs stained for PROX1, the LYVE1 signal was dim in some vessels, especially in LVs with valves around the FM and PPA, and also around the MMA (Fig. 1 D). Consequently, PROX1/LYVE1 double staining was used for meningeal LV characterization and analysis in both pups and adults.

Parasinusoidal meningeal LVs developed from LVs located alongside the jugular veins (JVs) and cranial nerves (CNs; IX–XI), which enter the skull via the jugular foramen next to the FM. At P3, the deep cervical LNs (dcLNs) were linked to LVs alongside the JVs (Fig. S1 B). Intracranially, the parasinusoidal LVs grew upwards dorsolaterally along the sigmoid sinus (SS), converging then along the transverse sinus (TS) to the superior sagittal sinus (SSS) and extending further toward the anterior part of the skull (Fig. 1 G). The growing front had reached the TS at P8, the confluence of the sinuses (COS) at P16, and the rostral end of the SSS at P28 (Fig. 1 G). The meningeal lymphatic vessels around the SSS remained thin and were occasionally discontinuous, even in adult mice. Approximate locations of the LVs along the dural sinuses and the direction of growth are indicated in Fig. 1 (A and B) and Fig. S1 A. From P16 onwards, further LVs were discovered also in the dura mater covering the cerebellum, in association with veins branching from the TS (Fig. S1 C). LVs in the dura, attached to the frontal bone overlying the olfactory bulb, and beside the rostral rhinal veins (RRV) became apparent at P16 and were well developed at P24 (Fig. 1 H), before the LVs along the SSS had reached the rostral area, indicating separate paths of growth for the LVs in the rostral and caudal parts of the skull.

Also in other parts of the skull base, meningeal LVs started to develop shortly after birth around the skull foramina along the CNs and associated BVs, and they were already well developed at P20 (Fig. S1, F–H). In the meninges under the olfactory bulb, some PROX1$^+$/LYVE1$^+$ lymphatic-like structures were visible at P2 around the external ethmoidal BVs (Fig. S1 F). The meningeal lymphatic vasculature overlying the cribriform plate next to olfactory nerve bundle (CN I) and associated internal ethmoidal BVs was evident before P8 (Fig. S1 G). These vessels formed an extensive lymphatic network around the cribriform foramina, piercing through the ethmoidal foramina and joining the nasal mucosal LVs that drain into the dcLNs (Walter et al., 2006; Aspelund et al., 2015; Lohrberg and Wilting, 2016). Rudimentary, discontinuous LVs were observed already at P0 around the CN III–VI bundle and associated BVs, whereas around the optic nerve (CN II), nerves close to the FM (CN VII-VIII) and their associated BVs, the LVs were evident slightly later, around P8 (Fig. S1 H). Extracranial LVs were also observed in the eye orbit after eye enucleation at P0 (Fig. S1 I).

At 1 mo of age (P28), the meningeal LVs were developed in all parts of the skull. Comparison of the *Prox1-eGFP* reporter mice at 1 mo and 2 yr of age revealed their similar patterning around BVs and cranial and spinal nerves (Fig. S2, A–D). In 2-yr-old mice, some enlarged LVs as well as more

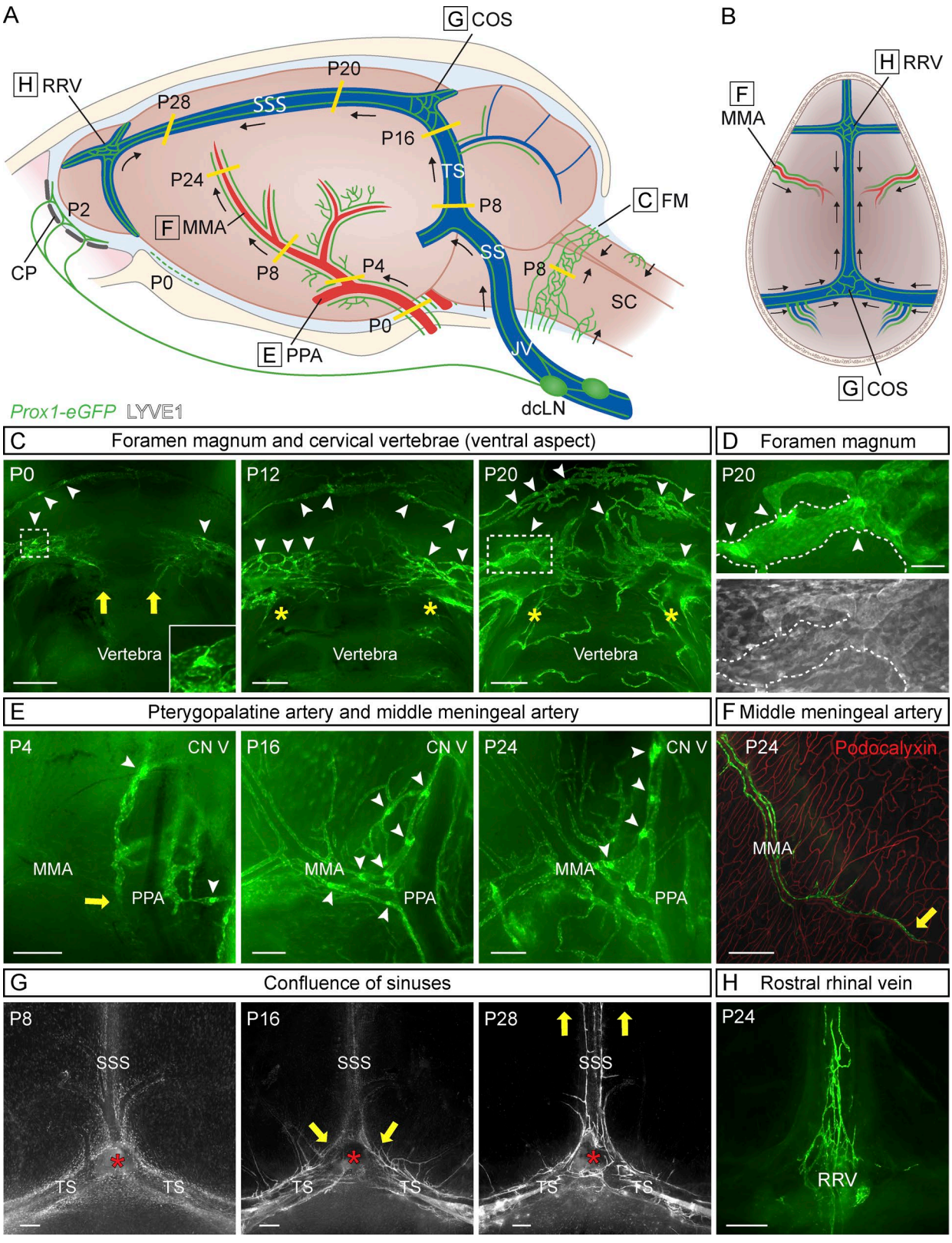

Figure 1. **Postnatal development of the meningeal lymphatic network.** (A and B) Schematic illustration showing meningeal LVs (green) superimposed on the corresponding anatomical structures at different postnatal (P) days (A) and the direction of LV growth (B). CN V, CN V (trigeminal nerve); CP, cribriform plate; SC, spinal cord. (C–H) Development of the meningeal lymphatic network, detected by *Prox1-eGFP* (green) reporter and LYVE1 immunostaining

disjointed and sparse lymphatic structures with fewer valves were observed, especially around the FM and PPA (Fig. S2, A and B). The presence of meningeal LVs was also confirmed in marmosets (Fig. S2 E).

Meningeal LVs around the spinal cord

At P4, some thin PROX1$^+$ LVs were observed in meninges overlying the vertebrae and intervertebral spaces after spinal cord removal (Fig. 2 E). Further LVs in spinal meninges developed concomitantly along the spinal nerves and associated BVs as the LVs were detected almost simultaneously in cervical, thoracic, and lumbar areas during the early postnatal period. These strongly PROX1/LYVE1/VEGFR3/podoplanin–positive and weakly CD31- and podocalyxin-expressing LVs extended to the midline, covering mainly the intervertebral area on both dorsal and ventral sides along the entire spinal canal (Fig. 2, A and D–G); valves were observed after P4 (Fig. 2, E and F, arrowheads). From P8 onward, the LVs covering the FM connected to meningeal LVs in the cervical spinal canal (Figs. 1 C and 2 E, yellow asterisks). On the ventral side of the spinal canal, the meningeal LVs did not connect at the midline, even in adult mice (Fig. 2 E), whereas on the dorsal side, they formed a connected uniform pattern by P16 that extended all the way to cisterna magna (CM; Fig. 2 F). The spinal meningeal LVs became caudally more elongated, adjusting to the growing vertebrae. On the dorsal side, the caudal LVs were also organized into a more circular pattern (Fig. 2 F). The LVs exited the spinal canal laterally together with the BVs and spinal nerves (Fig. 2 G and Fig. 3, A and B). LVs in the spinal meninges and their exit alongside the spinal nerves and BVs are illustrated in Fig. 2 (A–C) and Fig. 3 A.

Lymphatic sprout extension and cluster fusion contribute to meningeal lymphangiogenesis

In the early developmental stages, especially before and around P8, a considerable number of LYVE1$^+$/PROX1$^-$ cells were observed in areas where the meningeal LVs later developed (Fig. 1 G, Fig. 4 A, and Fig. S1, E–G and I). These cells expressed the macrophage mannose receptor CD206 and F4/80, suggesting that they were related to macrophages/microglia (Fig. 4 B, hereafter: macrophage-like cells). Upon further development of the LYVE1$^+$/PROX1$^+$ meningeal lymphatic vasculature, this LYVE1$^+$/PROX1$^-$ macrophage-like cell subpopulation was strongly decreased (Fig. 1 G, Fig. 4 A, and Fig. S1, F and G), although CD206$^+$/F4/80$^+$ cell density did not markedly decrease (Fig. 4 C). Interestingly, in adult mice, intracerebroventricularly (i.c.v.) injected fluorescent ovalbumin was found to accumulate into some of the CD206$^+$/F4/80$^+$/PROX1$^-$ macrophage-like cells along the meningeal LVs (Fig. S2 F).

Six hours after 5-ethynyl-2-dioxyuridine (EdU) administration to P16 pups, EdU-positive cells were evident near the tips of developing LVs (Fig. 4 G) and in discrete clusters of PROX1$^+$/LYVE1$^+$ LECs (Fig. 4 H) located around the developing LVs (Fig. 4, D and E; and Fig. S1, C, F, and G). These clusters were CD206/F4/80 negative; thus, they were not macrophage-like cells (Fig. 4, C and F). They formed filopodia that connected to the surrounding clusters and the already formed LVs (Fig. 4, D, E, and H), and they disappeared during later developmental stages, concomitantly with the formation of LVs, suggesting that they merged with the sprouting LVs. Interestingly, during the early postnatal period, PROX1$^+$/LYVE1$^-$ BVs were found in the areas where the LVs would later form (Fig. S1, D–G). The PROX1 fluorescence in the BVs disappeared during the formation of the PROX1$^+$/LYVE1$^+$ LVs and clusters. Furthermore, occasional cells in the PROX1 expressing BVs were weakly LYVE1 positive (Fig. S1 E, arrows).

VEGF-C, but not VEGF-D, is essential for meningeal LV development

Transgenic K14-VEGFR3-Ig mice expressing a soluble VEGF-C/D trap display aplasia of meningeal LVs, and embryos lacking both *Vegfc* alleles die before meningeal LVs start to develop (Karkkainen et al., 2004; Aspelund et al., 2015). Because of this, heterozygous *Vegfc*$^{LacZ/+}$ knockout mice were used in our analysis of meningeal LV development. *Vegfc*$^{LacZ/+}$ pups and adult mice had nearly complete absence of LVs in their meninges (Fig. 5 A; Fig. S3, A, and B; and Table S1), whereas the meningeal LVs in *Vegfd* gene–deleted mice were indistinguishable from those in WT control mice (Fig. 5 B; Fig. S3, D–F; and Table S1). When we deleted *Vegfc* in the *Rosa26-CreER*^{T2}*;Vegfc*$^{flox/flox}$; (*Vegfc*$^{i\Delta R26}$) mice by tamoxifen administration at P3–P5 or P8–P10, no LVs were found in the cranial or spinal meninges of the *Vegfc*$^{i\Delta R26}$ mice (Fig. 5, C and D; Fig. S3 G; and Table S1). To our surprise, littermate *Vegfc*$^{flox/flox}$ gene–targeted mice, but not *Vegfc*$^{flox/WT}$ mice, also had severely hypoplastic meningeal LVs, suggesting that the conditional allele leads to a hypomorphic phenotype (Fig. 5, C and D; and Fig. S3 G). *Vegfc* mRNA quantification indicated that the *Vegfc*$^{flox/WT}$, *Vegfc*$^{flox/flox}$, and *Vegfc*$^{i\Delta R26}$ mice express ∼75%, 50%, and 1% of the WT *Vegfc* mRNA levels, respectively (Fig. S3 H). This confirmed that the meningeal LVs are more sensitive to decreased *Vegfc* expression

(gray). Meningeal LVs around the FM at P0, P12, and P20 (C and D); around the PPA and MMA at P4, P16, and P24 (E); around the MMA at P24 (F; showing BV immunostaining for podocalyxin in red); around the COS at P8, P16, and P28 (G); and around the RRV at P24 (H). Dashed boxes in C (P0 and P20) surround the lymphatic valves magnified in C (P0) and D (P20). (D) Close-up of lymphatic valves (arrowheads) in the FM region at P20; note the lack of LYVE1 staining of collecting LVs (dashed line). Yellow lines in A and arrows in C and E–G point to the growing LV front. Arrowheads in C–E mark lymphatic valves. Asterisks in C indicate the connection between LVs around the FM and LVs around the spinal canal. Asterisks in G indicate remnants of the excised pineal gland. Data shown are representative of $n = 3–6$ per time point and staining. Bars: (C and F–H) 400 µm; (D) 100 µm; (E) 200 µm.

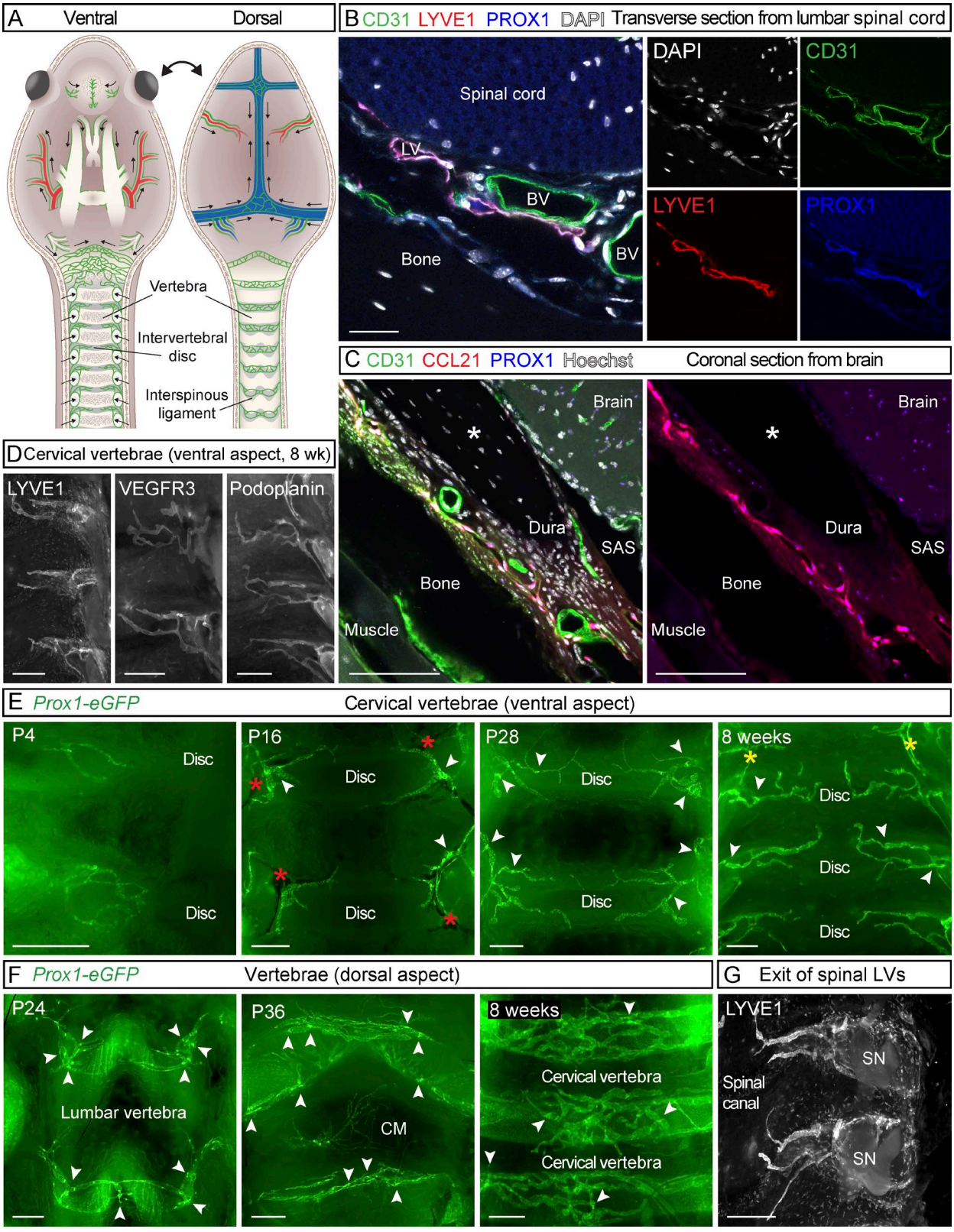

Figure 2. **LVs in spinal meninges.** (A) Schematic illustration of meningeal LVs (green) attached to the ventral and dorsal sides of the cranium and spinal canal after removal of the brain and spinal cord. SN; spinal nerve. (B) Transverse section of lumbar spine of an adult mouse showing LVs in dura, immunostained for CD31 (green), LYVE1 (red), and PROX1 (blue). (C) Coronal sections of adult skull showing the meningeal LVs, immunostained for CD31 (green),

than intestinal or cutaneous LVs (Nurmi et al., 2015). As in the WT pups during meningeal LV development (Fig. 1 G, Fig. 4 A, and Fig. S1, F, G, and I), the mice with absent or severely hypoplastic LVs had numerous LYVE1$^+$/CD206$^+$/F4/80$^+$ cells in the areas where the LVs were supposed to develop (Fig. 5, A, C, and D; and Fig. S3, A–C and G).

VEGF-C–expressing smooth muscle cells (SMCs) are located along the routes of LV growth

We next analyzed *Vegfc* gene expression around meningeal LVs by X-gal staining of tissues from the *Vegfc*$^{LacZ/+}$ heterozygous mice in which the *LacZ* gene, encoding β-galactosidase, has been inserted into the *Vegfc* locus (Karkkainen et al., 2004). At P21, prominent β-gal staining was detected in close proximity of the areas where the meningeal LVs were developing, especially around the dural venous sinuses, PPA, MMA, and BVs around the FM and CNs (Fig. 6, A–C and E). An intense signal was detected in the pineal (Fig. 6 A, asterisks) and pituitary (Fig. 6 D) glands. The blue staining around the vessels had a distinctive pattern (Fig. 6, A–C and E, arrowheads), resembling α-smooth muscle actin (αSMA) staining in SMCs that enwrap the arteries and veins (Fig. 6, F–H), suggesting that these cells constitute an important paracrine source of VEGF-C. The meningeal LVs were not coated by SMCs, but they were always found adjacent to the αSMA–positive arteries and veins in the pups and in adult mice, suggesting that VEGF-C from BVs guides LV development and maintenance. This hypothesis was further supported by the spatiotemporal relationship between the development of SMCs and LVs in the meninges. For example, in WT mice, the SSS displayed developing SMCs and no LVs at P6, whereas at P18, when LVs started to elongate along the SSS, an extensive SMC coverage was present (Fig. 6 F).

Vegfr3 deletion arrests meningeal LV development

The importance of VEGFR3 in meningeal LV development was assessed by postnatal gene deletion in *Rosa26-CreER*^{T2}*;Vegfr3*$^{flox/flox}$ mice (*Vegfr3*$^{i\Delta R26}$). This resulted in nearly complete lack of LVs in the cranial and spinal meninges at P21, confirming the critical role of VEGFR3 (Fig. 7, A and B; Fig. S4, A–C; and Table S1). In *Vegfr3*$^{i\Delta R26}$ pups, only a few rudimentary and segmented LV remnants were occasionally found near the PPA and FM (Fig. S4 C, arrowhead). Although the *Rosa26-CreER*^{T2} allele is also active in BV ECs, there were no obvious differences between the meningeal BVs of the *Vegfr3*$^{i\Delta R26}$ mice and their littermates at P21 (Fig. 7 B).

Blocking the VEGF-C–VEGFR3 interaction impairs meningeal LV development

To interfere with lymphangiogenic signals by using another method, we used the VEGF-C/D trap, which neutralizes both VEGFR3 ligands (Mäkinen et al., 2001). Adeno-associated viral vectors (AAVs) encoding soluble VEGFR3 (AAV–mVEGFR3$_{1-4}$-Ig, encoding the mouse "VEGF-C/D trap") or control vector (AAV–mVEGFR3$_{4-7}$-Ig) was injected i.p. to WT pups at P0, and the meninges were analyzed at P21, P70, and P200. The vector-encoded proteins were detected in serum 24 h after AAV injection into adult mice (Fig. 7 F). As in the globally *Vegfr3*-deleted mice, the LVs in the cranial and spinal meninges were atrophic at all three time points in mice expressing the VEGF-C/D trap (Fig. 7, C and D; Fig. S4, D–F; and Table S1). To confirm that the effect was local, the vectors were injected intracisternally (i.c.m.) to *Vegfr3:YFP* transgenic mice, which express the Venus fluorescent protein (YFP) under the control of *Vegfr3* regulatory sequences (Calvo et al., 2011). In these mice, strong YFP fluorescence in the vasculature colocalized with PROX1 immunofluorescence, confirming the strong YFP signal as a bona fide reporter of LECs (Fig. S5 I). AAV–mVEGFR3$_{1-4}$-Ig injection at P7 resulted in significantly reduced YFP$^+$ meningeal LVs at P14 (Fig. S5, A, B, and G), whereas meningeal BVs were not affected (Fig. S5, D, E, and H). Injection at P21, when meningeal LVs are already well developed but still growing, resulted in their complete absence around the dural sinuses 40 wk after gene transfer (Fig. 7 E), but some LVs persisted in the basal part of the skull and around the spinal cord (Fig. S4 G).

Growth of meningeal LVs in response to VEGF-C gene transfer

We next asked whether VEGF-C gene transfer can be used for the induction of meningeal lymphangiogenesis. First, AAV encoding mouse VEGF-C (AAV–mVEGF-C) or PBS (mock) was injected i.c.m. to *Vegfr3:YFP* mice at P7. When the dura mater attached to the parietal bones was analyzed at P14, a robust increase of the YFP$^+$/PROX1$^+$ signal corresponding to LVs was observed especially around the TS and COS, and in the area of the frontal bone (Fig. S5, A, C, G, and I), whereas BV growth was not affected (Fig. S5, D, F, and H). Enlarged and additional LVs and sprouts emanating from them were also observed by LYVE1 staining in adult C57BL/6J mice injected i.c.v. with the AAV–mVEGF-C versus AAV without payload (empty-AAV; Fig. 8, A–D).

The effect of VEGF-C on BBB integrity was analyzed by measuring Evans blue (EB) extravasation three hours after its i.v. injection into 12-wk-old mice treated 4 wk earlier

CCL21 (red), and PROX1 (blue). Asterisk indicates an artifactual space created during preparation. (D) LYVE1, VEGFR3, and podoplanin immunostaining of spinal meninges. (E and F) Development of the meningeal LVs in the spinal canal on the ventral (E) and dorsal (F) aspects during the indicated postnatal (P) days. (G) LVs exiting the spinal canal together with the spinal nerves. Arrowheads in E and F point to lymphatic valves, and red asterisks in E indicate BVs. Yellow asterisks in E indicate the connection between LVs around the FM and LVs around the spinal canal. Data shown are representative of n = 3–6 per time point and staining. Bars: (B) 20 µm; (C) 50 µm; (D, F, and G) 400 µm; (E) 300 µm.

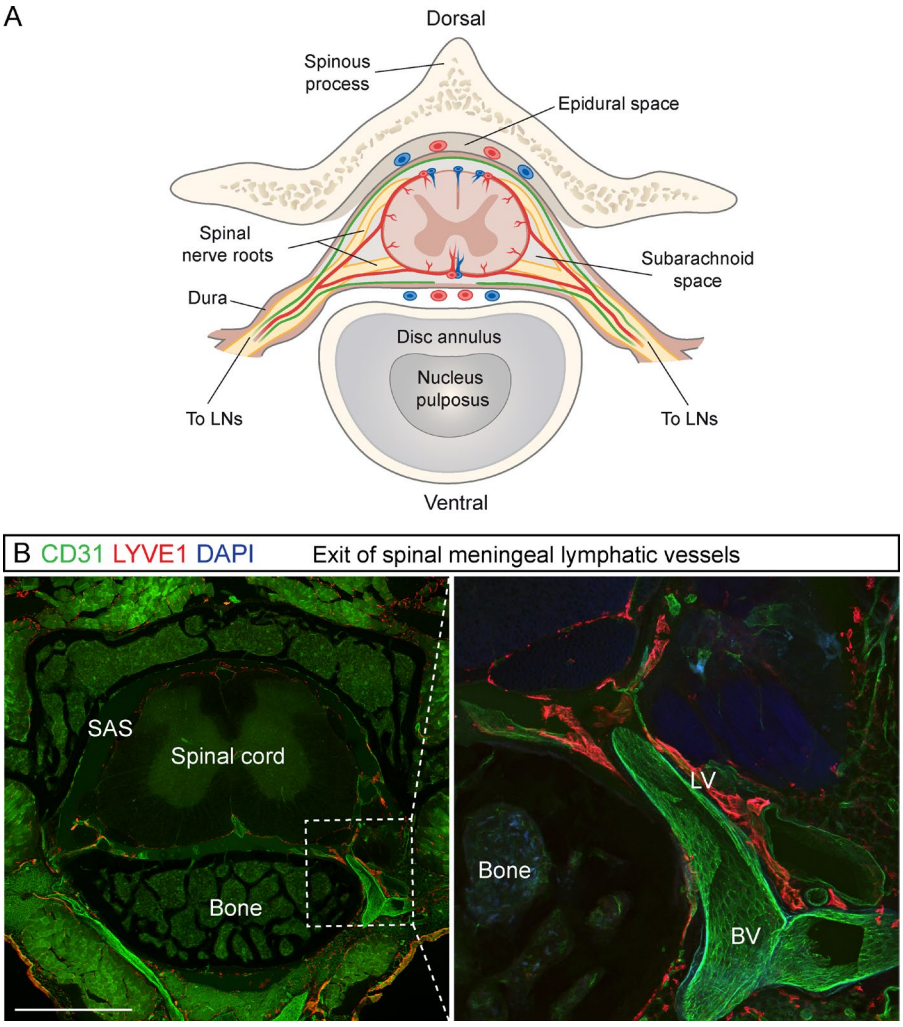

Figure 3. **LV exit from the spinal canal along the spinal nerves and BVs.** (A) Schematic transverse view of the spinal cord and its blood (red) and lymphatic (green) vessels. (B) Transverse section of spinal cord with a close-up showing the exit of the LVs and BVs along the spinal nerve bundle in LYVE1 (red) and CD31 (green) immunostaining, respectively (n = 3). Bar, 2 mm.

with i.c.m. injection of AAV–mVEGF-C or AAV–mVEGFR3$_{4-7}$-Ig (control). Intraperitoneally administered LPS (10 mg/kg) was used as positive leakage control. No significant differences were detected in the EB extravasation in mice treated with AAV–mVEGF-C (2.7 ± 0.89 µg/ml, n = 6) or AAV–mVEGFR3$_{4-7}$-Ig (2.5 ± 0.56 µg/ml, n = 5), whereas LPS induced BBB leakage (14.13 ± 6.98 µg/ml, n = 6; Fig. 8 E). Moreover, mice injected with AAV–mVEGF-C or control vector showed no significant differences in immunostaining of the adherens junction protein VE-Cadherin at BV EC junctions (Fig. 8 F). The results indicate that the i.c.m. injection or AAV–mVEGF-C did not cause BBB disruption.

Inhibition of VEGFR3 signaling leads to regression of meningeal LVs in adult mice

To determine whether continuous VEGFR3 signaling is required for meningeal LV maintenance, we deleted *Vegfr3* in adult mice by tamoxifen administration. 20 wk later, the *Vegfr3*$^{i\Delta R26}$ mice showed a significant regression of meningeal LVs when compared with tamoxifen-treated littermate *Vegfr3*$^{flox/flox}$ mice. Although the LVs around the dural sinuses had completely regressed (Fig. 9 A and Table S1), some isolated LVs were still observed in the meninges coating the basal part of the skull and the spinal canal (Fig. 9 B).

To avoid the developmental failure of most LVs that occurs in K14-VEGFR3-Ig mice, which lack lymphangiogenic signals in utero (Mäkinen et al., 2001; Aspelund et al., 2015), we instead blocked the VEGFR3 signal transduction pathway in adult mice by using the VEGF-C/D trap, which did not affect already established LVs in a previous study (Nurmi et al., 2015). We injected VEGF-C/D trap or control vector i.p. into 8-wk-old WT mice and analyzed the mice 1, 2, 5, and 8 wk thereafter. Meningeal LV regression was evident already after 1 wk of VEGF-C/D trap expression and progressed until the parasinusoidal LVs had disappeared from the top part of the skull (Fig. 9, C and E; and Fig. 10, B and H). Although some rudimentary LVs were occasionally detected around the dural sinuses even 8 wk after gene transduction, the regression was significant when compared with mice injected with control vector (Fig. 9, C and E; and Fig. 10, B and H). Vector delivery by i.c.v. injection caused an equally efficient regression of meningeal LVs around the dural sinuses 8 wk after injection

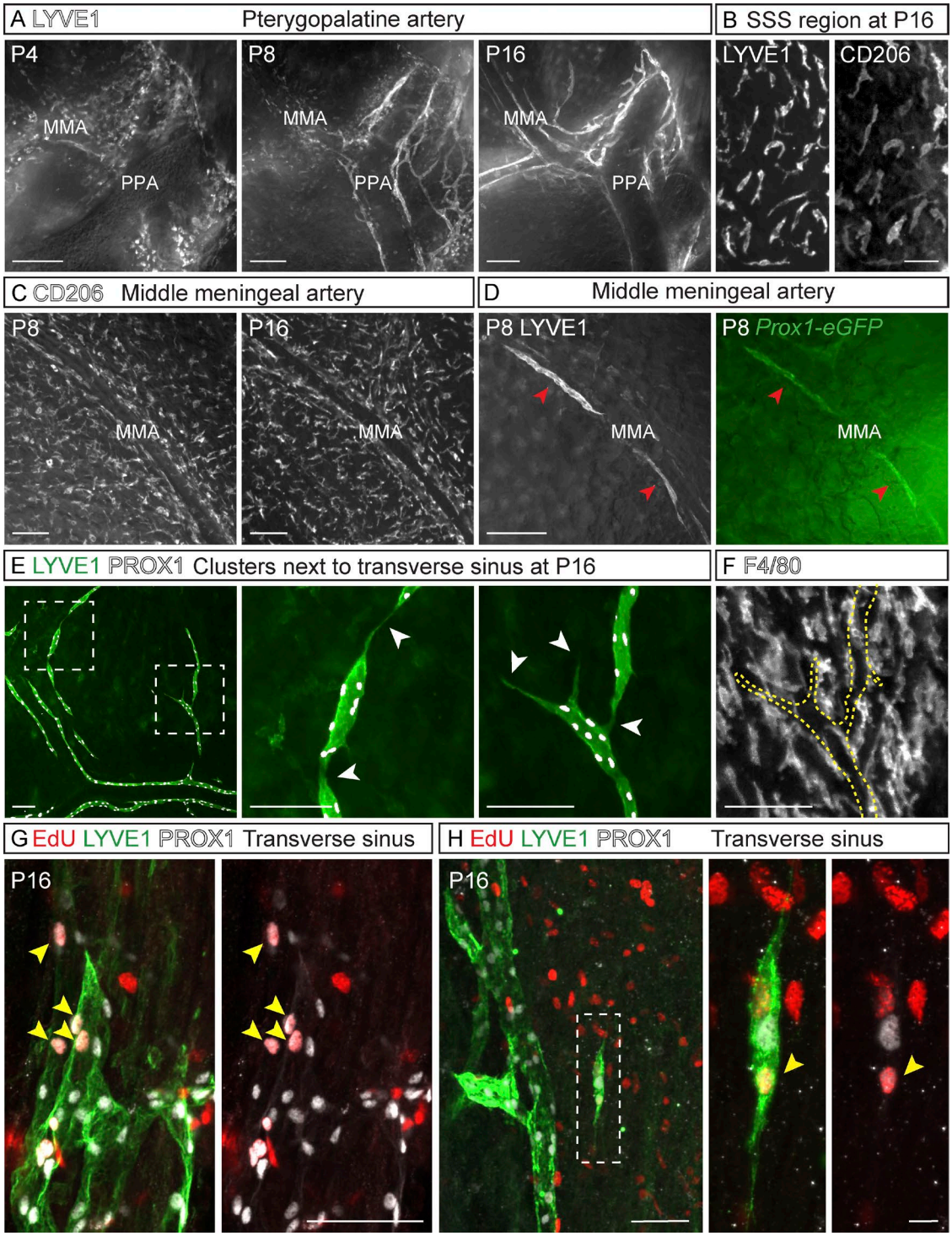

Figure 4. **Sprout extension and fusion of cell clusters in meningeal lymphangiogenesis.** (A) LYVE1 staining of LVs developing around the PPA. (B) LYVE1$^+$/CD206$^+$ macrophage-like cells around the SSS at P16. (C) CD206 immunostaining around the MMA. (D) LYVE1 (gray) and *Prox1-eGFP* (green)–positive cell clusters (arrowheads) around the MMA. (E) LYVE1 (green) and PROX1 (gray) immunostaining of LEC clusters around the TS at P16. Dashed boxes indicate areas of the close-up images shown in E. Arrowheads indicate connections of the clusters with each other and with the already-formed LVs. (F) F4/80 immunostaining of macrophage-like cells for comparison. Dashed line indicates the LEC clusters shown in E. (G and H) EdU-positive LECs (arrowheads in G) in the tip cell area around the TS and (H) in isolated clusters stained for PROX1 (gray) and LYVE1 (green). EdU was administered 6 h before tissue harvest. Data shown are representative of $n = 2–4$ per time point and staining. Bars: (A and D) 200 µm; (B, F, and G) 50 µm; (C and E) 100 µm; (H) 10 µm.

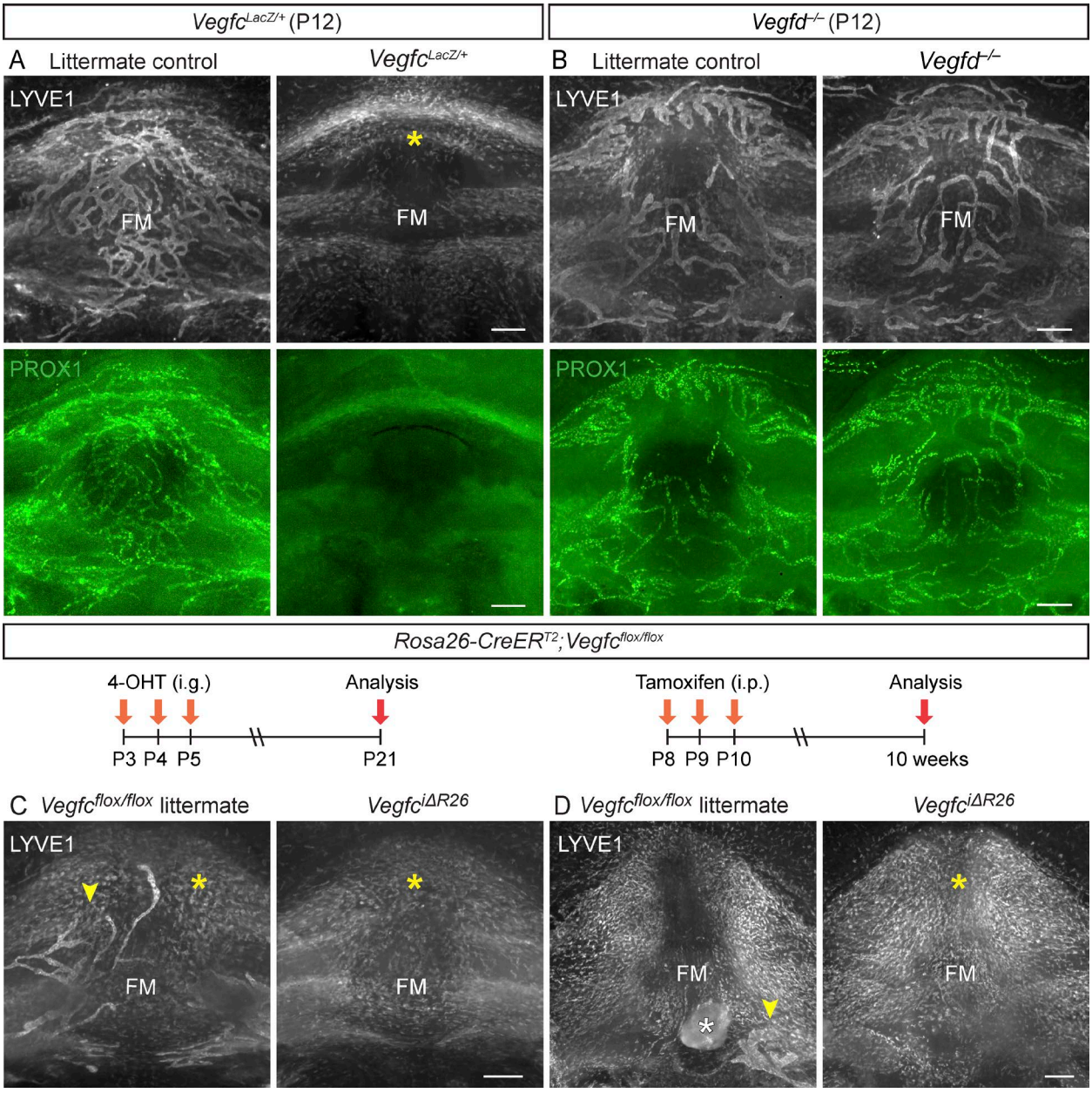

Figure 5. **VEGF-C, but not VEGF-D, is essential for normal meningeal LV development.** (A and B) LYVE1 (gray) and PROX1 (green) staining of the FM area in P12 *Vegfc*$^{LacZ/+}$ (n = 3, 3; P = 0.0429; A) and *Vegfd*$^{-/-}$ mice and their littermate controls (n = 3, 3; P = 0.2264; B). (C and D) Comparison of LYVE1 staining in the FM area in *Vegfc*$^{flox/flox}$ littermate controls and *Vegfc*$^{i\Delta R26}$ mice (C) at P21 (n = 3, 3; P = 0.4391) and (D) at 10 wk of age (n = 3, 6; P = 0.0457). The time course of 4-OHT or tamoxifen injections and analysis is illustrated above the images. Yellow (A, C, and D) and white (D) asterisks indicate LYVE1-positive macrophage-like cells and extra tissue left after dissection, respectively. Arrowheads point to LV fragments. Data shown are representative of two independent experiments using littermate mice. Student's t test was used to calculate p-values. Bars, 200 µm.

(Fig. 10, A, B, and H), whereas no significant loss of meningeal LVs occurred in the basal part of skull or in the spinal canal. Moreover, no significant differences were detected in EB extravasation in the brains of mice that were injected i.c.v. with AAV–VEGFR3$_{1–4}$-Ig (104 ± 19%), control AAV–mVEGFR3$_{4–7}$-Ig (95 ± 5%), or PBS (100 ± 11%, P > 0.05), whereas 10 mg/kg LPS induced BBB leakage (LPS, 123 ± 8%, P < 0.05 vs. PBS). These results indicated that neither i.c.v. injection nor vector administration causes BBB disruption.

The tyrosine kinase inhibitor sunitinib causes a reversible regression of meningeal LVs

The finding that the already established meningeal lymphatic vasculature in adult mice is uniquely dependent on

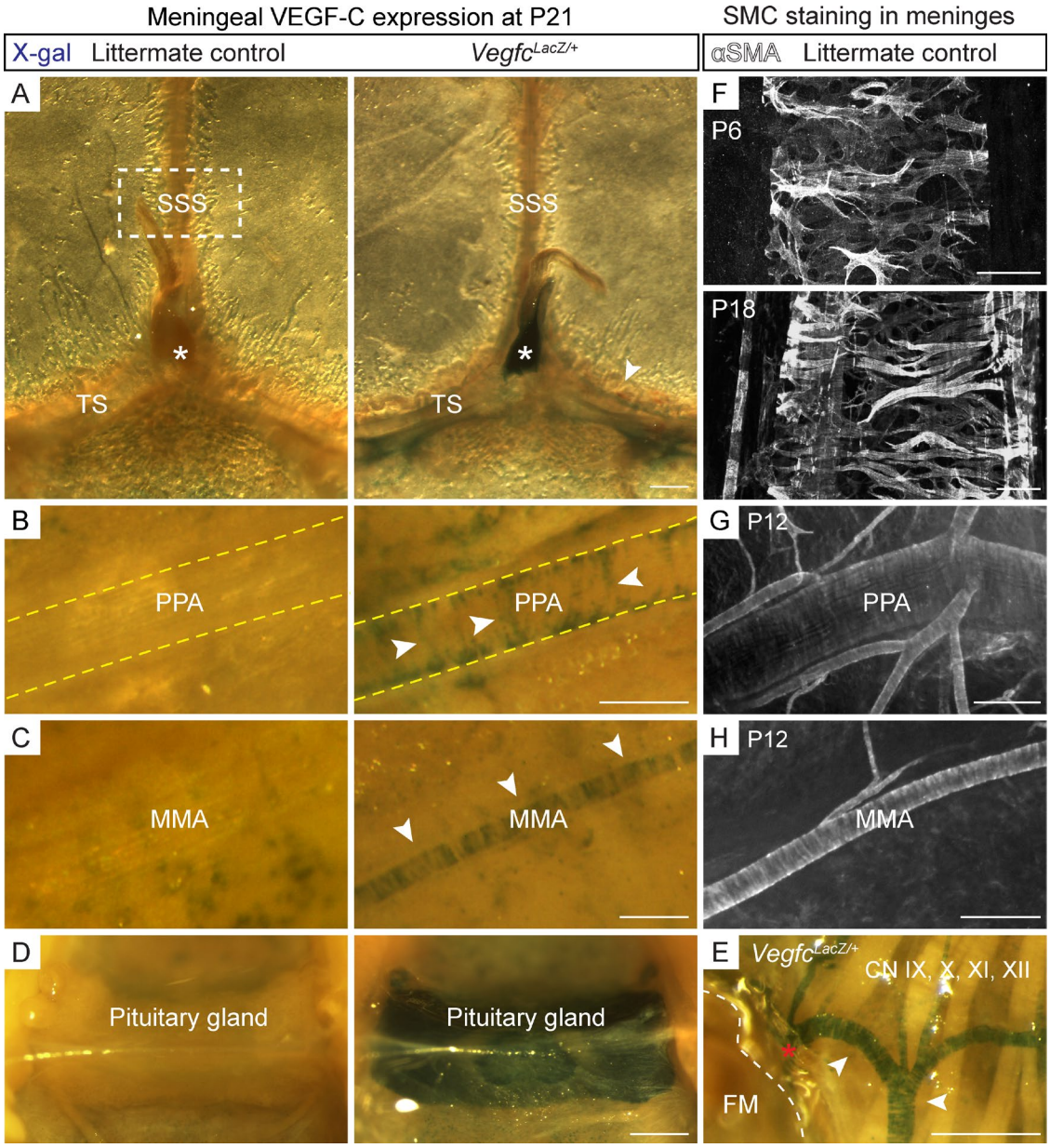

Figure 6. **Smooth muscle cells provide a vascular source of VEGF-C for meningeal LVs.** (A–E) β-Galactosidase staining of meningeal tissue showing VEGF-C expression around the TS and SSS and in the pineal gland (asterisks; A), PPA (B), MMA (C), pituitary gland (hypophysis; D), and FM (dashed line) and the CNs (E) in *Vegfc*$^{LacZ/+}$ mice at P21. Note the "stripe-like" pattern resembling the wrapping of SMCs around the BVs (arrowheads). The asterisk in E shows VEGF-C expressing meningeal BV that continues from the skull base to the spinal canal. (F–H) αSMA staining around the SSS from the boxed area in A at P6 and P18 (F), PPA at P12 (G), and MMA at P12 (H). Data shown are representative of $n = 2–4$ per time point and staining using littermate mice. Bars: (A) 400 µm; (B, E, and G) 200 µm; (C and H) 100 µm; (D) 500 µm; (F) 50 µm.

continuous VEGF-C–VEGFR3 signaling led us to investigate whether its regression occurs during treatment with sunitinib, a VEGFR tyrosine kinase inhibitor that is used for targeting tumor angiogenesis in cancer patients. At the 60 mg/kg dose, sunitinib inhibits VEGFR3 tyrosine kinase activity, but this did not affect pre-existing LVs in an earlier study (Nurmi et al., 2015). Surprisingly, we found that an acute 2-wk sunitinib treatment resulted in significant regression of parasinusoidal LVs, especially in the SSS region (Fig. 9, D and G). This regression was reversible upon cessation of sunitinib treatment, as some of the LVs had grown back 4 wk after sunitinib withdrawal (Fig. 9, D and H). This indicates that the meningeal lymphatic vasculature is plastic, being exceptionally sensitive to sunitinib treatment–induced regression in adult mice yet having the capacity to grow back after treatment.

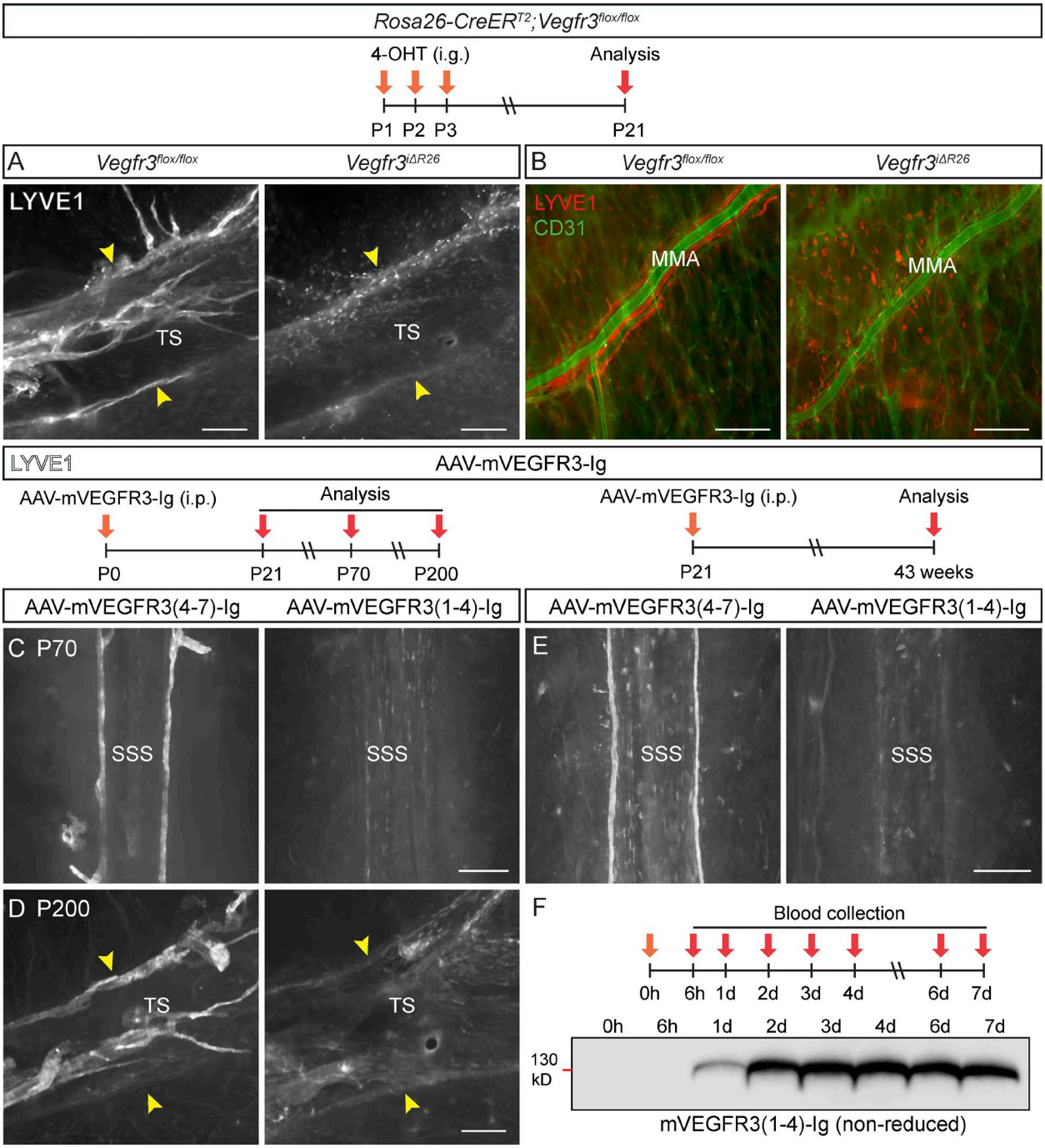

Figure 7. **VEGFR-3 is essential for meningeal LV development.** (A and B) Comparison of dural LYVE1 staining in P21 mice deleted of *Vegfr3* (*Vegfr3*^{iΔR26}, $n = 4$) and their littermate controls (*Vegfr3*$^{flox/flox}$, $n = 9$) around the TS (A) and MMA (B). BVs stained for CD31 (green). (C and D) LYVE1 staining around the SSS and TS in mice injected with the indicated AAVs at P0 and analyzed at P70 ($n = 6, 6$; C) or P200 ($n = 3, 3$; D). (E) LYVE1 staining around the SSS in mice injected with the same vectors on P21 and analyzed 40 wk later ($n = 7, 6$). The width of the TS is indicated by the arrowheads in A and D. (F) Western blot showing VEGFR3-Ig protein in serum of an individual mouse at the indicated time points after i.p. AAV injection. Data shown are representative of two independent experiments. Bars, 200 µm.

Inhibition of VEGFR3 signaling results in decreased CSF transport into the dcLNs

To test whether the interruption of VEGFR3 signaling affects CSF drainage function, mice were injected i.p. with VEGF-C/D trap or control vector at 8 or 3 wk of age. 8 or 40 wk later, respectively, the mice were subjected to a functional

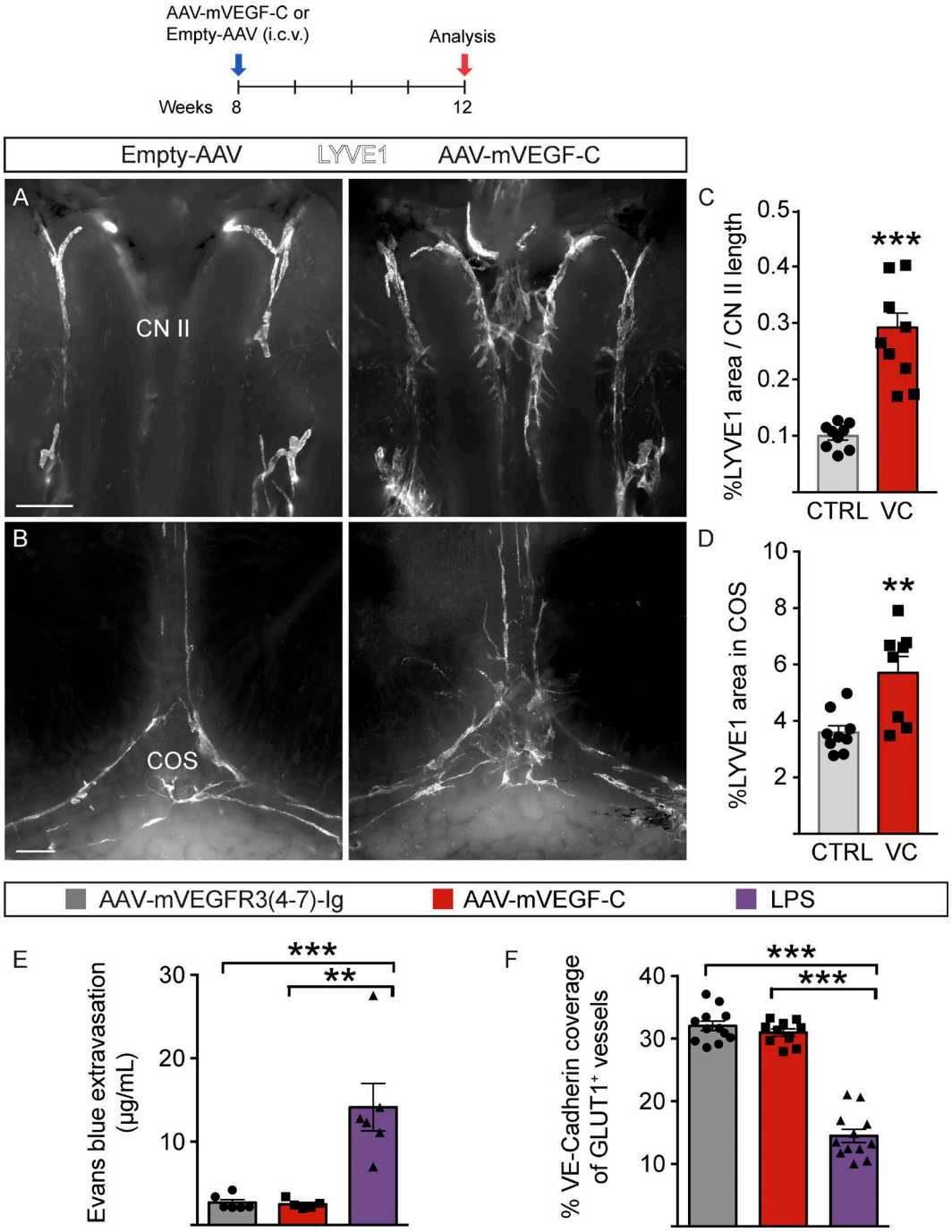

Figure 8. **Meningeal LV growth in response to AAV–mVEGF-C.** (A–E) Analysis of meningeal LVs in mice injected i.c.v. with AAV–mVEGF-C (n = 9) or AAV without payload (empty-AAV; n = 9). LYVE1 staining of the CN II (A) and COS area (B), and quantification of LYVE1 area-percentage per CN II length (C) and COS region (D). CTRL, Empty-AAV; VC, AAV–mVEGF-C. (E and F) Analysis of BBB integrity in 12-wk-old mice injected i.c.m. with AAV–mVEGF-C (n = 5) or AAV–mVEGFR3$_{4–7}$-Ig (control, n = 6) at 8 wk of age. Comparison is made to mice treated with i.p. LPS (n = 6). Quantification of EB extravasation into brain tissue 3 h after i.v. administration (E) and VE-Cadherin and BV-specific GLUT1 colocalization in brain sections (F). Data shown are representative of two independent experiments. A Student's t test was used to calculate p-values. **, P < 0.01; ***, P < 0.001. Values are expressed as mean ± SEM. Bars: (A) 100 µm; (B) 500 µm.

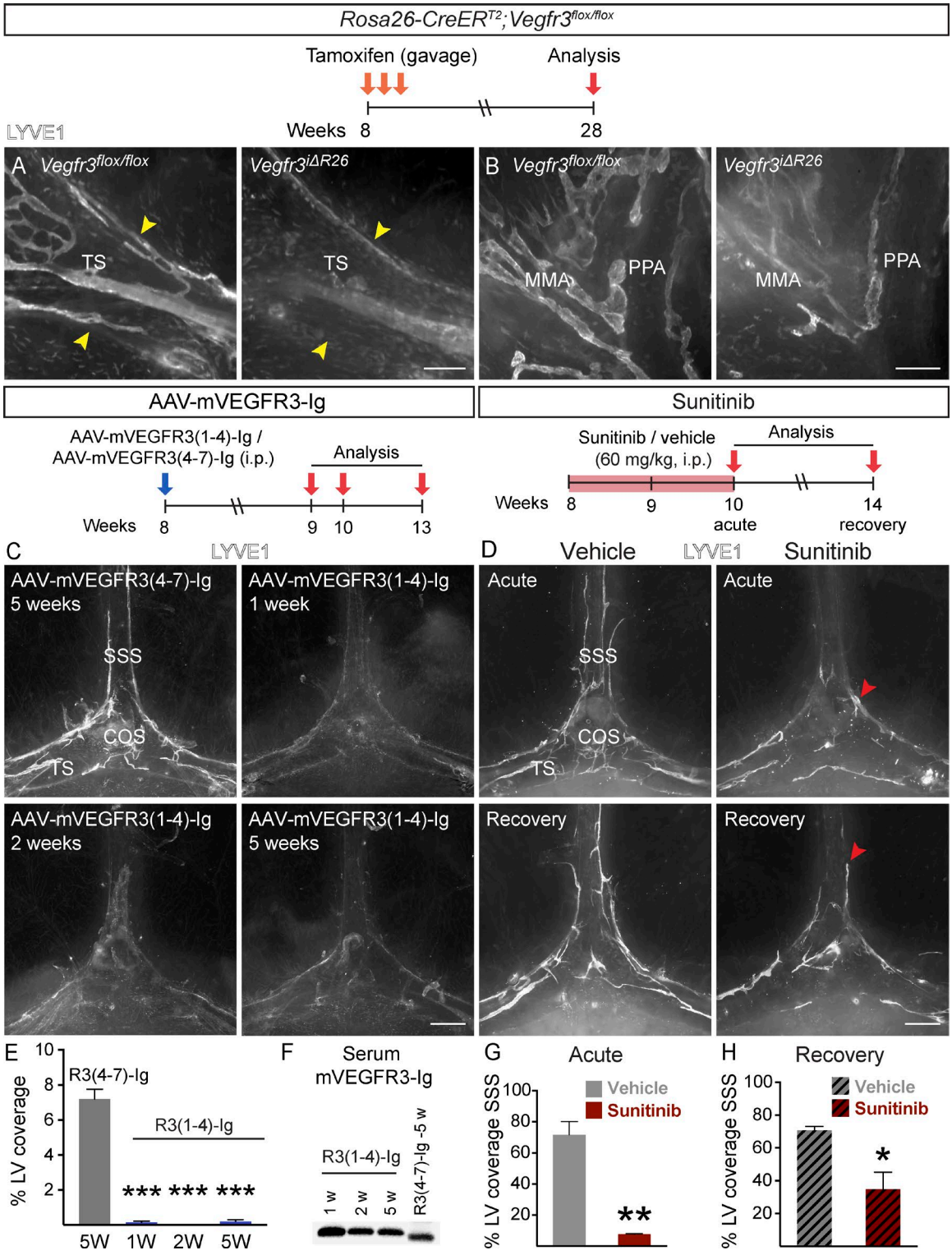

Figure 9. **VEGFR-3 signaling is required for LV maintenance in adult meninges.** (A and B) Comparison of LYVE1 staining around the TS (A) and PPA (B) in *Rosa26-Vegfr3*$^{flox/flox}$ (n = 4) and *Vegfr3*^{iΔR26} mice (n = 4) 20 wk after tamoxifen administration. Arrowheads indicate TS width. (C and D) LYVE1 staining around the COS (C) at the indicated time points after AAV–mVEGFR3$_{1–4}$-Ig or AAV–mVEGFR3$_{4–7}$-Ig injection (n = 3, 3 in each time point) and in mice administered daily with 60 mg/kg sunitinib (D) and analyzed as indicated (n = 3, 3 in both time-points). Arrowheads point to the rostral end of the LV front in acute and recovery phases. (E) Quantification of the LV area in the experiment shown in C. (F) Western blot showing mVEGFR3-Ig protein in serum

assay evaluating i.c.v.-injected 500-nm microsphere transport from the CSF space into dcLNs (Fig. 10 F). The microspheres were chosen as an indicator of CSF exit pathway as opposed to fluorescently labeled ovalbumin, which tended to accumulate into $CD206^+/F4/80^+$ macrophage-like cells covering the $LYVE1^+$ LVs in adult mice (Fig. S2 F). The meningeal LVs along the dural sinuses had regressed at both time points (Figs. 10, B, C, and H; and Fig. 7 E); at 40 wk, LVs in the spinal meninges and at the base of the skull had also regressed (Fig. S4 G). In both experimental setups, the VEGF-C/D trap caused also a strong reduction of microsphere transport from the lateral brain ventricle to the dcLNs (Fig. 10, D, E, and I).

DISCUSSION

Our results show that in mice, essentially all intracranial and spinal meningeal LVs develop during the first postnatal month, starting at the base of the skull by extension of sprouts and fusion of LEC clusters located beside pre-existing BVs and CNs. VEGF-C, which was essential for LV development, was produced most prominently by vascular SMCs and the pituitary and pineal glands. Meningeal LVs could be induced to grow further in postnatal and adult mice by using intracranial delivery of a viral vector producing exogenous VEGF-C. Inhibition of VEGF-C–VEGFR3 signaling using VEGF-C or VEGFR3 gene targeting, VEGF-C/D trap, or a clinically approved VEGFR tyrosine kinase inhibitor resulted in developmental arrest and gradual regression of the meningeal LVs in pups and in adults, respectively. Furthermore, meningeal lymphatic regression was associated with decreased clearance of i.c.v.-injected microspheres into extracranial LNs.

Most LVs in adult tissues are formed during embryonic development, with the exception of the Schlemm's canal in the eye and lacteal vessels in the gut (Kim et al., 2007; Aspelund et al., 2014; Nurmi et al., 2015). Meningeal LVs developed still later, during the first postnatal month. In comparison, the development of the CNS BVs in mice begins in the embryonic stage with the formation of the perineural vascular plexus at E7.5–E8.5, followed by capillary sprout invasion into the neuroepithelium by angiogenesis in a caudal to cranial order at midgestation, followed by recruitment of pericytes, and continuing with a gradual development of the BBB (Lindahl et al., 1997; Mancuso et al., 2008). Development of intracranial and spinal meningeal LVs started around the various foramina at the base of the skull and spinal canal within a short time interval after birth, proceeding along the BVs and cranial and spinal nerves and appearing latest in the anterior part of the SSS in the top part of the skull. 4 wk after birth, the meningeal LVs already formed an extensive network with numerous sprouts that covered all parts of the cranium and persisted in similar locations in 2-yr-old mice. Interestingly, SMCs were absent, but valves were present in the meningeal LVs from the early time point of their development, particularly in the basal parts of the skull and around the spinal cord. This suggests that the meningeal lymphatic network consists of initial and precollector LVs. The mainly basal distribution of valves indicates that the meningeal LVs are exposed to different flow conditions and possess distinct functional properties in various regions around the CNS.

The spinal meningeal LVs developed postnatally almost simultaneously in the cervical, thoracic, and lumbar regions instead of a successive cranial-caudal order. This suggests that, similarly to the intracranial LVs, growth along the nerves and BVs occurs against the direction of lymph flow in the subsequent functional LVs. The completed spinal LV network was connected to the LVs around the FM on both dorsal and ventral sides, covering mainly the intervertebral disc area on the ventral side and the interspinous ligament area on the dorsal side, and extending out from the spinal canal laterally in association with the spinal nerves and BVs. The spinal meningeal LV patterning changed along the ventral–dorsal and cranial–caudal axes of the spine, which may reflect LV site-specific functional properties. Studies in several animal species have indicated that up to half of extracranial CSF drainage occurs via the lymphatic pathway (Pollay, 2010). Besides the CSF drainage via cranial outflow pathways into extracranial LVs, functional connections of the spinal SAS with the lymphatic system have been also descibed previouly (Brierley and Field, 1948; Field and Brierley, 1948; Zakharov et al., 2003). Interestingly, i.c.v.-injected tracers have been reported to accumulate only partially into lumbar and intercostal LNs, whereas lumbar and intrathecal administrations resulted in tracer accumulation mainly in lumbar plus intercostal LNs and mandibular plus truncal LNs, respectively (Boulton et al., 1996, 1998; Kwon et al., 2017), indicating regional specificity of CSF drainage. Therefore, modulating spinal meningeal LVs and their function could provide possibilities for manipulation of the exit of CSF, macromolecules, and cells in conditions such as spinal cord injury, multiple sclerosis, and syringomyelia.

The development of meningeal LVs along BVs and nerves occurred by sprouting lymphangiogenesis, but isolated LEC clusters of variable size also seemed to form vessel-like structures, similar to the clusters of incompletely known origin (Klotz et al., 2015; Martinez-Corral et al., 2015; Stanczuk et al., 2015). These isolated clusters proliferated, formed filopodia and connected to other clusters and to the sprouting lymphatic vessels. Their variable size suggests that they are formed by an ongoing process during a transient developmental phase. Furthermore, their disappearance later on suggests that they are intermediate structures that incorporate into the sprouting LVs. $PROX1^+/LYVE1^-$ BVs occurred

at the indicated time points after AAV injection. (G and H) Quantification of SSS length covered by LVs in sunitinib-treated mice in the acute phase (G) and recovery phase (H). Data shown are representative of two independent experiments. A Student's *t* test was used to calculate p-values. *, $P < 0.05$; **, $P < 0.01$; ***, $P < 0.001$. Values are expressed as mean ± SEM. Bars: (A) 200 µm; (B) 150 µm; (C and D) 500 µm. W, weeks.

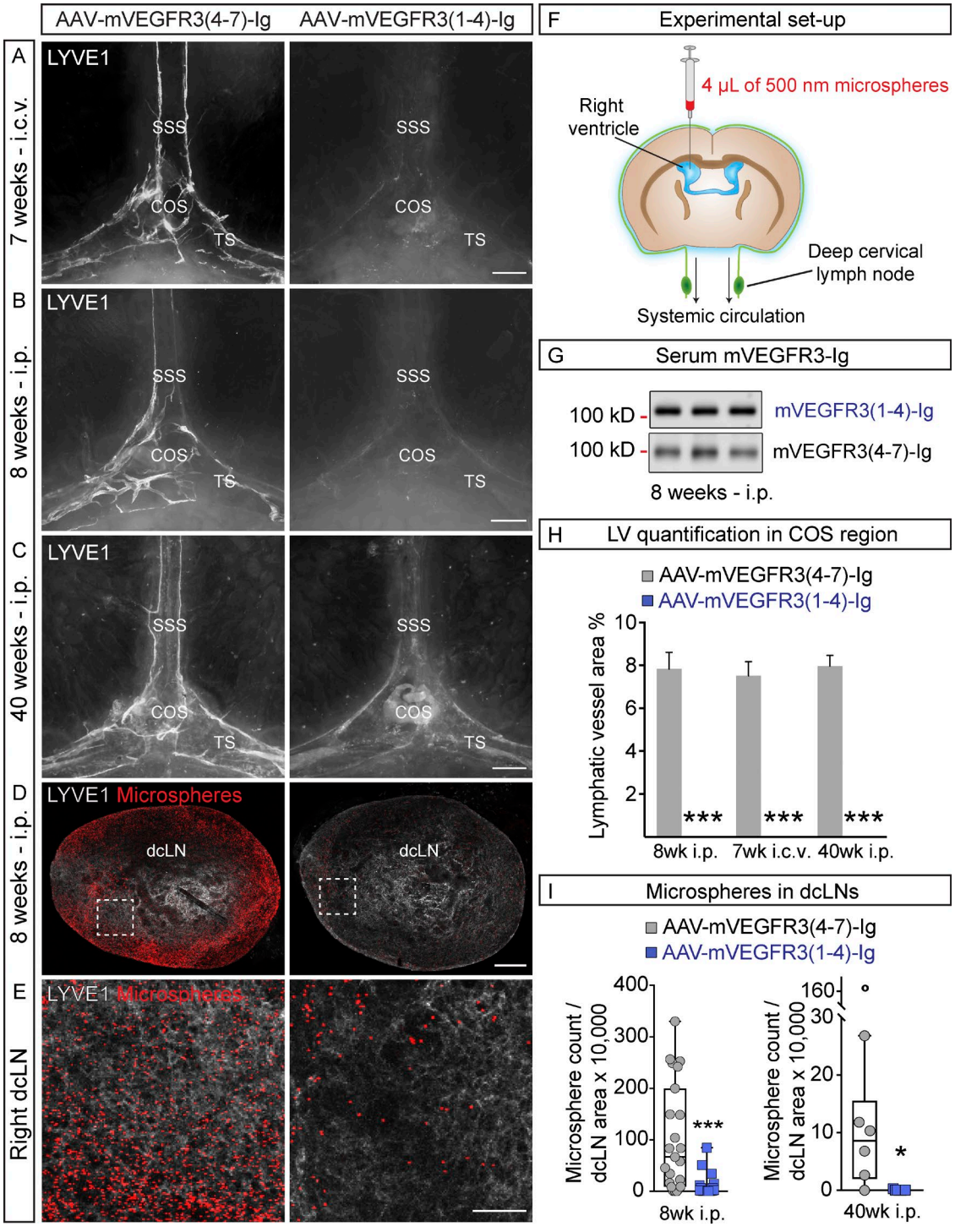

Figure 10. **Regression of meningeal LVs decreases drainage of i.c.v.-injected microspheres.** (A–C) Representative images of LYVE1-stained LVs around the COS 7 wk after i.c.v. injection (A; *n* = 6, 6), 8 wk after i.p. injection (B; *n* = 6, 6), and 40 wk after i.p. injection (C; *n* = 7, 6) of the indicated AAVs into 9-, 8-, and 3-wk-old mice, respectively. (D) Representative images of LYVE1–stained dcLNs (gray) containing fluorescent microsphere (red) in mice subjected to the functional assay schematically described in F. Analysis was done 8 wk after i.p. injection of the indicated AAVs into 8-wk-old mice (*n* = 12, 12). (E) Representative close-up images of the boxed areas in D. (G) Western blot showing mVEGFR3-Ig protein in serum 8 wk after i.p. AAV injection. (H) Quantification of LVs in the experiments shown in A–C. (I) Quantification of the number of microspheres in dcLNs, normalized to dcLN area in the experiments shown in B–E. Data shown are representative of two independent experiments. A Student's *t* test was used to calculate p-values. *, $P < 0.05$; ***, $P < 0.001$. Values are expressed as mean ± SEM. Bars: (A–C) 500 µm; (D) 200 µm; (E) 50 µm.

in the same areas where the first meningeal LVs would later form. The gradual disappearance of PROX1$^+$ BVs and the coincidental appearance of PROX1$^+$/LYVE1$^+$ LEC clusters and LVs is consistent with the possibility that at least some of the LVs are derived directly from BVs, reminiscent of the development of the first LVs in midgestation embryos (Oliver and Alitalo, 2005; Hägerling et al., 2013). The observation of weakly stained LYVE1$^+$ cells in the PROX1$^+$ BVs further suggests that the LEC clusters in the early postnatal meninges could be BV-derived (Oliver and Alitalo, 2005). Further genetic lineage tracing should be used to map the origin and fate of the clusters and meningeal LVs.

An abundant LYVE1$^+$/PROX1$^-$/CD206$^+$/F4/80$^+$ macrophage-like cell subpopulation was associated with the developing LYVE1$^+$/PROX1$^+$ LVs, disappearing gradually during further LV development, perhaps because of *Lyve1* down-regulation. Such cells were again observed when meningeal LV development was arrested in pups or their regression induced in adults upon VEGF-C–VEGFR3 signaling interference, which inhibits LEC growth and survival (Mäkinen et al., 2001). The LYVE1$^+$/CD206$^+$/F4/80$^+$ macrophage-like cells may promote LV growth by secreting growth factors (e.g., VEGF-C), or they may transdifferentiate into LECs that integrate into the growing LVs, hence disappearing during later developmental stages (Schoppmann et al., 2002; Kerjaschki, 2014). The CD206$^+$/F4/80$^+$ macrophage-like cells that persisted and coated LYVE1$^+$ LVs in adult mice accumulated i.c.v.-injected ovalbumin, suggesting that at least part of the tracer associated with the meningeal LVs is taken up by these cells. This is interesting, as CD206 is an endocytic receptor for ligands of microbial and endogenous origin and involved in antigen delivery that may contribute to T cell differentiation and activation (Martinez-Pomares, 2012). The recently identified cd206$^+$/lyve1$^+$/prox1$^+$ paravascular and selectively phagocytotic cell population (muLEC, BLEC, or FGP cells) in zebrafish brain resembles both CD206$^+$ macrophage-like cells and LECs (Bower et al., 2017; van Lessen et al., 2017; Venero Galanternik et al., 2017), although the zebrafish cells do not appear to form LVs. Further work should elucidate whether these cells share analogous functions with the LYVE1$^+$/CD206$^+$/F4/80$^+$ cells we observed in mouse meninges. Further studies should also resolve the tracer-specific CNS exit pathways including meningeal LVs and the conserved and divergent properties of the associated phagocytes attached to them along the arteries and veins. In fact, part of fluorescent macromolecules that accumulated along meningeal LVs after intracerebral injection may reside in such cells (Aspelund et al., 2015).

As previously reported for cutaneous LVs (Karkkainen et al., 2004), we found severe hypoplasia of the meningeal LVs in heterozygous *Vegfc* knockout mice, whereas *Vegfd* knockout mice showed no LV phenotype or *Vegfc* up-regulation (Honkanen et al., 2016). This indicates that *Vegfd* is dispensable for meningeal lymphatic development. By analysis of a series of mice with hypomorphic *Vegfc* alleles, or their conditional deletion, we estimate that at least 50–75% of the WT level of *Vegfc* mRNA is required for normal meningeal lymphatic development. Thus, the meningeal LVs are considerably more sensitive to decreased *Vegfc* expression than cutaneous or intestinal LVs (Nurmi et al., 2015). Consistent with the mostly gravitational down flow of lymph from the cephalic region, the meningeal LVs appeared to be devoid of SMCs and thus of lymphangions typical for collecting LVs. However, the LVs were located in close proximity to the blood vascular SMCs, which appeared to be also the main source of VEGF-C in the meninges. Unlike pial BVs, dural BVs develop postnatally, and VEGF-C levels have been reported to rise during SMC differentiation in vitro, which, together with proteolytic activation of VEGF-C, may regulate the timing of meningeal LV development (Mack et al., 2009; Jeltsch et al., 2014). Strong VEGF-C expression was also found in the pituitary and pineal glands, which may provide hubs for coordination of the meningeal LV and endocrine BV development. Although the VEGF-C production in SMCs most certainly guides the development of meningeal LVs, factors involved in VEGF-C activation (CCBE1, ADAMTS3, and possibly other proteases) and those produced by blood vascular SMCs, such as CXCL12, probably also contribute to their development (Cha et al., 2012; Jha et al., 2017).

Although expression of VEGF family ligands via viral vector injection directly into mouse brain parenchyma produces dose-dependent vessel leakage (Gaál et al., 2013), the i.c.v. injection of AAV–VEGF-C stimulated meningeal lymphangiogenesis without blood vascular side effects in the meninges or BBB. However, the spinal meningeal LVs were not affected by i.c.v. injection of AAV–VEGF-C in pups or adult mice, suggesting either that they are less sensitive to VEGF-C than cephalic LVs or that the VEGF-C concentration in the spinal meninges was insufficient after i.c.v. delivery of the vector. Further studies should address whether different administration routes, concentrations, or longer periods of VEGF-C expression lead to maturation and increased drainage function of newly generated LVs, as shown for the functional reconstitution of LVs after LN evacuation in mouse axilla (Tammela et al., 2007).

Global deletion of *Vegfr3* in pups led to nearly complete lack of the meningeal LVs; only minor LV fragments persisted in the basal part of the cranium. Neonatal administration of VEGF-C/D trap resulted in complete and sustained loss of meningeal LVs inside the cranium and the spinal canal. Administration at P21 led to similar loss of LVs next to dural sinuses, but only partial LV atrophy at the skull base and in the spinal canal. VEGF-C/D trap administration to adult mice led to a prolonged depletion of the parasinusoidal LVs, which regressed within days after blocking of the VEGFR3 signal transduction pathway. The order in LV development thus seems to inversely correlate with LV stability, so that the newly developed vessels are the most vulnerable ones to depletion of growth factor signals.

VEGFR signaling inhibitors are currently used in cancer therapy because most antiangiogenic VEGFR tyrosine kinase inhibitors target all three members of the VEGFR family (Welti et al., 2013). It was thus of interest to study whether clinically used VEGFR inhibitors induce lymphatic regression in the meninges. We chose to use sunitinib, which has been approved as a treatment of renal cell carcinoma and gastrointestinal stromal tumor (Faivre et al., 2007). A sunitinib dosage that inhibits all VEGFRs has been reported to cause pruning of blood capillaries in several tissues (Kamba et al., 2006). Sunitinib administration led to a significant reduction of the LV coverage in only 2 wk, particularly in vessels flanking the SSS. Interestingly, the LVs recovered partially during a 4-wk period after the termination of drug dosing. Despite the partial regrowth of the LVs after sunitinib withdrawal, even a transient lack of these vessels could have consequences (e.g., neurological symptoms in patients who undergo sunitinib treatment). In this regard, it should be noted that sunitinib has several side effects, some of which (such as fatigue and anorexia) could originate from CNS dysfunction (Aparicio-Gallego et al., 2011). Sunitinib treatment is usually intermittent but long-term. If LV pruning occurs in sunitinib-treated patients, drug holidays of sufficient length should allow their regrowth. Interestingly, drug adherence was significantly higher in metastatic renal cell cancer patients who received sunitinib according to the standard schedule (50 mg, 4 wk on and 2 wk off) than in patients who received sunitinib with more frequent but shorter drug holidays (Atkinson et al., 2014). Such patients also better tolerated the drug and had fewer severe adverse events, which often lead to discontinuation of the treatment.

Our novel findings showing the unique dependence of adult meningeal LV maintenance on VEGF-C–VEGFR3 signaling should thus provide means to create mouse models that lack LVs selectively in the cranial meninges and that have a functional decline in CSF transport. Hence, a selective meningeal LV ablation should be feasible when all other LVs have been formed (Karpanen et al., 2006; Nurmi et al., 2015). Moreover, as the K14-VEGFR3-Ig transgenic mice lacking LVs in several tissues show autoimmune features (Mäkinen et al., 2001; Card et al., 2014), our results provide an improved new model involving conditional deletion or functional blocking of VEGFR3 in adult mice and a tool to ablate the meningeal LVs without affecting the development of the immune system. This should be of particular interest in studies of neuroinflammation. For example, the effect of interruption of lymphatic transport on antigen presentation in draining LNs needs to be carefully analyzed. Selective meningeal LV deletion using these new tools should provide a novel understanding of the role of meningeal LVs in health and disease.

As the aforementioned results and considerations indicate, meningeal LVs are also present in primates, and the VEGF-C/D–VEGFR3 pathway possesses significant potential for therapeutic targeting of the CNS. Besides its ability to induce LV growth, VEGF-C is known to stimulate the contractile activity of SMCs around collecting LVs (Gogineni et al., 2013). Furthermore, as drugs that affect the contractile activity of collecting LVs can increase CSF outflow (Kim et al., 2014), increasing meningeal LVs and their drainage capacity by lymphangiogenic growth factor stimulation could provide therapeutic benefits for patients with Alzheimer's disease, stroke, or traumatic brain injury. VEGF-C gene therapy is already being used to treat lymphedema patients in phase 1 clinical trial (NCT02994771). The design of a safe and specific way of promoting therapeutic lymphatic expansion and improved outflow of fluid, cells, and macromolecules from the CNS could thus be possible if, for example, spatial and temporal control of the delivery and proteolytic activation of VEGF-C can be achieved. Future studies should aim at determining whether improving the function of meningeal LVs could be used in the prevention or treatment of different neuropathological conditions.

MATERIALS AND METHODS

Study approval

The study was approved by the Committee for Animal Experiments of the District of Southern Finland. The experiments performed at Yale were approved by the Institutional Animal Care and Use Committee of Yale University.

Mice and genetic deletions

The *Prox1-eGFP* (backcrossed six to eight times to C57BL/6JOlaHsd background mice; Choi et al., 2011), *Vegfc*$^{LacZ/+}$ (Hsd:ICR(CD-1); Karkkainen et al., 2004), *Vegfd*$^{-/-}$ (C57BL/6J; Baldwin et al., 2005), *Vegfc*$^{flox/flox}$ (C57BL/6J; Aspelund et al., 2014), *Vegfr3*$^{flox/flox}$ (C57BL/6J; Haiko et al., 2008), *Rosa26-CreER*^{T2} (C57BL/6J; Ventura et al., 2007), and BAC *Vegfr3:YFP* (C57BL/6J; Calvo et al., 2011) transgenic mouse lines have been previously described. Littermate mice were used as controls. For WT analysis, C57BL/6J or C57BL/OlaHsd background mice were used.

In the conditional mice (*Vegfc*$^{i\Delta R26}$, *Vegfr3*$^{i\Delta R26}$, and their Cre-negative littermates), gene deletions were done according to different experimental protocols depending on the age and experimental setting. For analysis at P21, P1–P5 mice received intragastric (i.g.) injections 2.5 µl/day of 25 mg/ml 4-OH-tamoxifen dissolved in ethanol (Sigma-Aldrich). Because 4-OHT administration for *Vegfc*$^{i\Delta R26}$ mice at the early postnatal time points causes ascites and can compromise survival, the mice analyzed at 10 wk of age received 30 µl/day of a 4 µl/26 µl 4-OHT-ethanol/sunflower oil mixture i.p. during P8–10 (Pitulescu et al., 2010). 8-wk-old *Vegfr3*$^{i\Delta R26}$ mice were treated with three consecutive i.g. doses of 20 mg/ml tamoxifen (Sigma-Aldrich, MO) dissolved in 100 µl corn oil.

Tissue preparation

Mice were given a lethal dose of ketamine and xylazine and perfusion-fixed through the left ventricle with ice-cold 1% paraformaldehyde (PFA) in PBS or with PBS only (for *Prox1-eGFP* mice) after puncture of the right auricle. Head

dissection was done by insertion of a fine pair of scissors to the CM and by cutting along the lines of the parietal bone until the rostral part was reached on both sides. The parietal bone was then removed carefully, taking extra care not to harm the attached dura mater. For the basal part of the skull, the brain was carefully removed and spinal canal was opened by making incisions alongside the lateral sides of the spinal canal. Extra care was taken that the surgical tools do not come close to the FM area or the ventral and dorsal parts of the spinal canal. The dissected tissues were immediately immersed in ice-cold 4% PFA, fixed overnight at +4°C, washed in PBS, and processed for staining.

Whole-mount staining and cryoimmunostaining

For whole-mount staining of the meninges, the fixed tissues were permeabilized with 0.3% Triton X-100 in PBS (PBS-TX) at room temperature (RT) and blocked with 5% donkey serum/2% bovine serum albumin/0.3% PBS-TX (DIM). Primary antibodies were diluted in DIM, and samples were incubated in the primary antibody mix at least overnight at 4°C. After washes with PBS-TX in RT, the tissues were incubated with fluorophore-conjugated secondary antibodies in PBS-TX overnight at 4°C, followed by washing in PBS-TX at RT. After postfixation in 1% PFA for 5 min, after washing with PBS, the stained samples were transferred to PBS containing 0.05% sodium azide (NaN_3) at 4°C and imaged as soon as possible.

For whole-mount staining of the dcLNs, the whole-mount protocol was used, as described in the previous paragraph, with an additional day of incubation with the primary antibodies. LNs were mounted with Vectashield mounting medium (Vector Laboratories) between two thin cover glasses without applying any extra pressure, sealed with Cytoseal 60 (Thermo Fisher Scientific), and imaged immediately.

For the whole-mount preparations of skullcaps of *Vegfr3:YFP* mice, P14 mice were perfused with 2% PFA solution, and the heads were fixed in 4% PFA for 24 h at 4°C and incubated in PBS with 5% sucrose for 5–6 d at 4°C (until they sunk to the bottom of the tube). For immunolabeling, skullcaps were incubated in PBS containing 5% donkey serum and 2% Triton X-100 for 2 h at RT, followed by incubation with primary antibodies in PBS containing 3% donkey serum and 0.2% Triton X-100, overnight at 4°C. After washing with 0.2% PBS-TX three times, the skullcaps were incubated with fluorophore-conjugated secondary antibodies in PBS with 3% donkey serum for 2 h at RT. After three washes with 0.2% PBS-TX, skullcaps were flattened by making incisions in the lateral parts, mounted with fluorescent mounting medium (Dako), sealed with Cytoseal 60, and left to dry with hairpin clamps.

For floating sections of the brain in the BBB experiment, 1-mm-thick brain sections of the second hemisphere were obtained using a vibratome. Sections were incubated in PBS containing 5% donkey serum and 2% Triton X for 2 h at RT, followed by overnight incubation with primary antibodies in PBS with 3% donkey serum and 0.2% Triton X at 4°C. After washing with 0.2% PBS-TX three times, the sections were incubated with fluorescent dye–conjugated secondary antibodies in PBS with 3% donkey serum for 2 h at RT. After three washes with 0.2% PBS-TX, the sections were mounted with fluorescent mounting medium (Dako) between a glass slide and cover glasses.

For cryosections of the skull and spinal canal, the fixed tissues underwent decalcification with 0.5 M EDTA, pH 7.4, at 4°C. When the bone was soft, samples were washed thoroughly with PBS and immersed in PBS containing 20% sucrose and 2% polyvinylpyrrolidone for 24 h at 4°C, embedded in OCT compound (Tissue-Tek), and frozen for storage at −80°C. 50–100-µm-thick sections were cut using a cryostat (Microm HM 550/CryoStar NX70; Thermo Fisher Scientific), air-dried, encircled with a pap pen, permeabilized with 0.3% PBS-TX, washed with PBS, and blocked in DIM at RT. After overnight primary antibody incubation at 4°C in DIM, the sections were washed with PBS and incubated with the appropriate fluorophore-conjugated secondary antibodies diluted in 0.3% PBS-TX for 1–2 h at RT. After washes with PBS, the sections were postfixed with 1% PFA for 5 min at RT, washed with PBS, mounted with Vectashield mounting medium (Vector Laboratories), sealed with Cytoseal 60, and imaged as soon as possible.

X-gal staining

For X-gal staining of skulls, *Vegfc*$^{LacZ/+}$ mice were perfused transcardially with ice-cold PBS. Collected tissues were fixed with 0.2% glutaraldehyde and stained with β-galactosidase substrate X-gal (Promega) using a previously published protocol (Karkkainen et al., 2004).

Marmoset dura

Marmoset skullcaps with the attached meninges were provided by the Deutsches Primatenzentrum GmbH, Leibniz Institute for Primate Research in Göttingen, Germany and Biomedical Primate Research Centre in Rijswijk, Netherlands. For whole-mount immunostaining, the meninges were carefully peeled off from the parietal bone, pinned onto a silicon plate, and stained with the common whole-mount protocol for meninges described above.

EdU proliferation assay

P16 mice were given an i.p. injection of 5 mg/ml EdU (in 100 µl) in 0.9% saline. 6 h later, the mice were sacrificed as described in the Tissue preparation section. For EdU detection, the Click-iT Alexa Fluor 594 Assay kit (Invitrogen) was used according to the manufacturer's protocol.

Antibodies

The following primary antibodies were used for immunostaining of mouse tissues: rat anti–mouse CD31 (1:500; clone MEC 13.3, BD), goat anti–mouse podocalyxin (1:500, AF1556; R&D Systems), chicken anti-GFP (1:300, ab13970;

Abcam), rabbit anti–mouse PROX1 (1:200; Petrova et al., 2008), goat anti–human PROX1 (1:200, AF2727; R&D Systems), polyclonal rabbit anti–mouse LYVE1 (1:1,000; Karkkainen et al., 2004), rat anti-mouse LYVE1 (1:300, MAB2125; R&D Systems), polyclonal goat anti–mouse VEGFR3 (1:50, AF743; R&D Systems), goat anti-CCL21 (1:500; R&D Systems), Syrian hamster anti–mouse podoplanin (1:50, 8.1.1-s; DSHB), rabbit anti-αSMA (1:400, ab5694; Abcam), goat anti–mouse CD206 (1:400, AF2535; R&D Systems), rat anti–mouse F4/80 (1:300, MCA497R; Bio-Rad/AbD Serotec), mouse anti-Glut1 (1:400; Abcam) and goat anti–VE-Cadherin (1:400, AF-1002; R&D Systems). For the marmoset meninges, mouse anti–human CD31 (1:400; DAKO), and goat anti–human PROX1 (1:200, AF2727; R&D Systems) were used. The primary antibodies were detected with the corresponding Alexa Fluor 488–, 594–, or 647–conjugated secondary antibodies (1:500, except for *Vegfr3:YFP* skullcaps and floating sections of the brain in 1:1,000; Molecular Probes/Invitrogen).

AAV transduction

For i.p. AAV transduction, adult C57BL/6JOlaHsd mice (8–10 wk) received a single i.p. dose (10^{12} viral particles in 200 µl) of a recombinant AAV encoding the ligand binding domains 1–4 of VEGFR3, fused to the IgG Fc domain (AAV–mVEGFR$3_{1–4}$-Ig; Fang et al., 2016). Control mice received AAV encoding the domains 4–7 of VEGFR3 (that do not bind VEGF-C or VEGF-D) fused to the IgG Fc domain AAV–mVEGFR$3_{4–7}$-Ig (Alitalo et al., 2013).

For i.c.v. AAV transduction, a single dose (10^{10} viral particles per mouse in 4 µl) of AAVs encoding VEGF-C (Anisimov et al., 2009) or AAV–mVEGFR$3_{1–4}$-Ig was injected i.c.v. into adult male C57BL/6JOlaHsd mice of 8–9 wk of age. Control mice received the same number of particles of AAV without payload or AAV–mVEGFR$3_{4–7}$-Ig, respectively. Mice were anesthetized with isoflurane (induction 4%, maintenance 2%) and placed in a stereotactic apparatus (Stoelting). AAV injections were conducted unilaterally into the lateral ventricle (A/P: 0.3; M/L: 1.0; D/V −2 mm below dural surface). A small burr hole was drilled with a micromotor drill (Stoelting). Intracranial injections were done with the aid of the mouse brain atlas of Paxinos and Franklin (Paxinos and Franklin, 2001), using a 33-G, 10-µl microsyringe (NanoFil; World Precision Instruments). A stereotactic microinjector (Stoelting) was used (flow rate 0.5 µl/min, volume 4 µl), and after completion of each injection, the needle was kept in place for 4 min in order to minimize backflow of the AAV solution. 5.0 mg/kg carprofen (administered subcutaneously) was used to relieve postoperative pain, and lidocaine was used as a local anesthetic.

For AAV transduction via an i.c.m. injection, *Vegfr3:YFP* pups (P7) were anesthetized by i.p. injection of 50 mg/kg ketamine and 5 mg/kg xylazine, after which a single 2-µl dose (10^9 viral particles per microliter) of AAV–VEGF-C, AAV–mVEGFR$3_{1–4}$-Ig, or PBS (mock) was injected into the CM using a Hamilton syringe with a 34-G needle and flow rate of 0.5 µl/min. PBS was used as a control. The needle tip was retracted 2 min after the injection. The pups were euthanized at P14 using an overdose of isoflurane.

The AAVs of serotype 9 were produced by the AAV Gene Transfer and Cell Therapy Core Facility, HiLIFE, University of Helsinki (He et al., 2005; Bry et al., 2010).

BBB leakage assay

To measure BBB integrity, an EB leakage assay was performed as previously published (Heinolainen et al., 2017) with the following modifications. Mice with the indicated AAV treatments were anesthetized with 50 mg/kg ketamine and 5 mg/kg xylazine and injected i.v. with 100 µl of 3% EB in PBS. After 1 h, mice were terminally anesthetized and perfused via intracardiac delivery of 25 ml ice-cold PBS. The brains were halved in sagittal plane, weighed, and minced in 500 µl of deionized formamide. Mice that were used as positive controls for BBB leakage were injected with 10 mg/kg LPS (from *Escherichia coli* 0111:B4; Sigma-Aldrich) i.p. 3 h before the EB administration.

Sunitinib treatment

Sunitinib treatment was performed as previously described (Nurmi et al., 2015). In brief, 8-wk-old male C57BL6/OlaHsd mice were administered 60 mg/kg sunitinib (Sutent; Pfizer) diluted in vehicle (1.8% NaCl, 0.1% Tween 20, and 0.5 carboxymethyl cellulose) or vehicle daily via oral gavage (i.g.) for 2 wk. The acute group was euthanized and analyzed immediately after this period. The rest of the mice were left to recover for 4 wk and analyzed thereafter.

i.c.v. tracer injections

For the microsphere drainage assay, the mice were anesthetized by i.p. injection of 100 mg/kg ketamine and 10 mg/kg xylazine in saline and prepared for i.c.v. injection as descibed in the AAV transduction section. 500 nm fluorescent microspheres (FluoSpheres carboxylate red; Invitrogen) were blocked with 1% BSA for 1 h, washed in PBS three times, and finally diluted 1:250 in artificial CSF (Perfusion fluid; M Dialysis AB). A 33-G WPI needle (World Precision Instruments) attached to a stereotactic microinjector (Harvard Apparatus) was slowly lowered to the right lateral ventricle coordinates (A/P: −0.34; M/L: 1.0 D/V: −2.5 mm below dural surface) and kept in place for 2 min before starting the injection. 4 µl of diluted microspheres was injected into the right lateral ventricle at the rate of 0.5 µl/min. The needle was slowly retracted 4 min after the injection, the skin was closed with metallic clips and the mice were placed into a warm chamber to recover. After 3 h, the mice were terminally anaesthetized, perfused with 1% PFA, tissues were harvested and processed for whole mount staining, as indicated in the Tissue preparation section.

For the A647-OVA uptake into meningeal LVs, 4 µl of 5 mg/ml A647-OVA (Molecular Probes) in sterile PBS was injected as described in the previous paragraph. After 2 h, the

mice were terminally anesthetized, perfused with 1% PFA, tissues were harvested and processed for whole mount staining.

Microscope image acquisition, processing, and analysis

Fluorescent stereo micrographs of stained samples were obtained by using an Axio Zoom.V16 fluorescence stereo zoom microscope (Carl Zeiss) equipped with an ORCA-Flash 4.0 digital sCMOS camera (Hamamatsu Photonics) or an OptiMOS sCMOS camera (QImaging). The ZEN 2012 software (Carl Zeiss) was used for image acquisition. Image brightness and contrast were adjusted using ImageJ (Version 1.50g, National Institutes of Health) or Photoshop (Version CS5, Adobe) software. Quantitative analysis was done using ImageJ software. $PROX1^+/LYVE1^+$ meningeal LVs were detected and quantified semiautomatically using Fiji software and AngioTool (Zudaire et al., 2011). Highlighted LVs were measured and reported as area fraction of region of interest.

Laser scanning confocal micrographs of the fluorescently labeled skull and spinal canal cryosections and dcLNs flat mounts were performed using a Carl Zeiss LSM 780 confocal microscope (air objectives 10× Plan-Apochromat with NA 0.45 and 20× Plan-Apochromat with NA 0.80, oil objective 40× Plan-Neofluar with NA 1.3) with multichannel scanning in frame. Zen 2011 software (Carl Zeiss) was used for image acquisition. The resulting micrographs were rendered to maximum intensity projections. For the dcLNs, the LN area was outlined based on LYVE1 staining. The number of beads within the LNs was quantified using Fiji software and reported relative to LN size.

Laser scanning confocal micrographs of the fluorescently labeled brain and whole-mount skullcap preparations of *Vegfr3:YFP* mice were acquired using a Leica TCS SP8 confocal microscope (air objectives 10× Plan-Apochromat with NA 0.45 and 25× Plan-Apochromat with NA 1.1) with multichannel scanning in-frame. LV area was measured using Fiji software and reported relative to total skullcap area, which was measured with the same software by encircling the visible skull area. For BV branching and area quantification, the CMM Analyser Software developed by N. Elie was used (Koch et al., 2011).

Western blotting

$VEGFR3_{1–4}$-Ig and $VEGFR3_{4–7}$-Ig proteins in serum were detected by Western blotting of 0.5-µl serum samples collected at the indicated time points. Mouse VEGFR3 domains 1–4 and 4–7 were detected with polyclonal goat anti–mVEGFR3 antibodies against the extracellular domain of VEGFR3 (1:1,000, AF743; R&D Systems).

Quantitative real-time PCR

Pituitary gland (hypophysis) samples were harvested from PBS-perfused mice and snap frozen in liquid nitrogen. Total RNA was extracted using TRIsure (Bioline) with phenol-chloroform followed by column isolation using Nucleospin RNA kit (Macherey Nagel) following the manufacturer's instructions. cDNA was synthesized from 500 ng total RNA using the High Capacity Reverse Transcription kit (Applied Biosystems). Quantitative real-time PCR was performed using the following primer pairs: *Vegfc-F*: 5′-GAG GTCAAGGCTTTTGAAGGC-3′; *Vegfc* reverse: 5′-CTG TCCTGGTATTGAGGGTGG-3′; *36b4* forward: 5′-GGA CCCGAGAAGACCTCCTT-3′; *36b4* reverse: 5′-GCACAT CACTCAGAATTTC-3′. Quantitative PCR reactions were performed with FastStart SYBR green master mix (Roche) and a BIO-RAD C1000 Thermal cycler according to a standardized protocol, and gene expression fold changes were calculated using the $2^{-\Delta\Delta CT}$ method.

Statistical analysis

All experiments were repeated at least twice, unless otherwise stated. All values are expressed as mean ± SEM. Quantitative data between two groups were compared with unpaired, two-tailed Student's *t* test; a Welch correction was applied for groups with unequal variances. Comparisons between three or more groups were done using one-way ANOVA with Tukey's post hoc test. Statistical analyses were done using GraphPad Prism V7.0 for MacOSX (GraphPad Software). Differences were considered statistically significant at $P < 0.05$.

Online supplemental material

Fig. S1 shows the postnatal development of the meningeal lymphatic network. Fig. S2 shows meningeal LVs in aged mice and marmosets and uptake of ovalbumin into macrophage-like cells beside the meningeal LVs. Fig. S3 shows that VEGF-C, but not VEGF-D, is necessary for normal meningeal LV development. Fig. S4 shows additional images for the requirement of VEGFR-3 for meningeal LV development. Fig. S5 shows the effects of inhibition or stimulation of VEGF-C–VEGFR3 signaling on the growth of meningeal LVs. Table S1 shows the statistical data for quantifications for the indicated panels in the main figures.

ACKNOWLEDGMENTS

We thank Krista Heinolainen and Laurent Jacob for help with the experiments; Emilia A. Korhonen, Kari Vaahtomeri, Riikka Kivelä, and Teemu Aitta-Aho for helpful discussions; Dr. Björg V. Pauling and Dr. Kerstin Mätz-Rensing from Deutsches Primatenzentrum GmbH, Leibniz Institute for Primate Research, Göttingen, Germany, and Dr. Bert A. 't Hart and Dr. Yolanda S. Kap from Biomedical Primate Research Centre, Rijswijk, Netherlands, for providing the marmoset meninges; and Dr. David Jackson for providing LYVE1 antibodies. We also thank Katja Salo, Mari Jokinen, Ville Hyvönen, Anni Näsi, Jarmo Koponen, Tanja Laakkonen, Tapio Tainola, and the personnel of the Laboratory Animal Center of the University of Helsinki for excellent technical assistance and gratefully acknowledge the expert help we received from the AAV Gene Transfer and Cell Therapy Core Facility and Biomedicum Molecular Imaging Unit.

This work was supported by the Jane and Aatos Erkko Foundation, the European Research Council (European Union Horizon 2020 research and innovation program, grant 743155), the Wihuri Foundation, the Academy of Finland (Centre of Excellence Program 2014-2019, grants 271845 and 307366), the Sigrid Juselius Foundation (all to K. Alitalo), Institut National de la Santé et de la Recherche Médicale

(J.-L. Thomas), Agence Nationale Recherche (grant 13-BSV4-0002-01), and the National Institutes of Health (grant R01EB016629-01 to J.-L. Thomas and grant R01 EY025979-01 to A. Eichmann). S. Antila was supported by the Biomedicum Helsinki Foundation, the Finnish Medical Foundation, Duodecim, the Orion Research Foundation, and the Finnish Cultural Foundation. S. Karaman was supported by the Swiss National Science Foundation (advanced postdoc mobility grant P300PB_164732). M. Airavaara was supported by the Academy of Finland (grant 250275) and the Finnish Funding Agency for Innovation (Tekes, 3iRegeneration). M.H. Voutilainen was supported by the Academy of Finland (grant 277910) and the Jane and Aatos Erkko Foundation. M. Saarma was supported by the Sigrid Juselius Foundation.

The authors declare no competing financial interests.

Author contributions: S. Antila and K. Alitalo conceived the study. S. Antila, S. Karaman, H. Nurmi, and K. Alitalo designed the experiments. S. Antila, S. Karaman, H. Nurmi, M. Airavaara, M.H. Voutilainen, T. Mathivet, D. Chilov, Z. Li, T. Koppinen, J.-H. Park, S. Fang, and A. Aspelund performed the experiments. S. Antila, S. Karaman, H. Nurmi, and T. Mathivet analyzed and interpreted data. M. Saarma, A. Eichmann, and J.-L. Thomas supervised research and provided funding. S. Antila, S. Karaman, and K. Alitalo wrote the manuscript.

Submitted: 1 March 2017

Revised: 22 September 2017

Accepted: 12 October 2017

REFERENCES

Alitalo, K. 2011. The lymphatic vasculature in disease. *Nat. Med.* 17:1371–1380. https://doi.org/10.1038/nm.2545

Alitalo, A.K., S.T. Proulx, S. Karaman, D. Aebischer, S. Martino, M. Jost, N. Schneider, M. Bry, and M. Detmar. 2013. VEGF-C and VEGF-D blockade inhibits inflammatory skin carcinogenesis. *Cancer Res.* 73:4212–4221. https://doi.org/10.1158/0008-5472.CAN-12-4539

Anisimov, A., A. Alitalo, P. Korpisalo, J. Soronen, S. Kaijalainen, V.M. Leppänen, M. Jeltsch, S. Ylä-Herttuala, and K. Alitalo. 2009. Activated forms of VEGF-C and VEGF-D provide improved vascular function in skeletal muscle. *Circ. Res.* 104:1302–1312. https://doi.org/10.1161/CIRCRESAHA.109.197830

Aparicio-Gallego, G., M. Blanco, A. Figueroa, R. García-Campelo, M. Valladares-Ayerbes, E. Grande-Pulido, and L. Antón-Aparicio. 2011. New insights into molecular mechanisms of sunitinib-associated side effects. *Mol. Cancer Ther.* 10:2215–2223. https://doi.org/10.1158/1535-7163.MCT-10-1124

Aspelund, A., T. Tammela, S. Antila, H. Nurmi, V.M. Leppänen, G. Zarkada, L. Stanczuk, M. Francois, T. Mäkinen, P. Saharinen, et al. 2014. The Schlemm's canal is a VEGF-C/VEGFR-3-responsive lymphatic-like vessel. *J. Clin. Invest.* 124:3975–3986. https://doi.org/10.1172/JCI75395

Aspelund, A., S. Antila, S.T. Proulx, T.V. Karlsen, S. Karaman, M. Detmar, H. Wiig, and K. Alitalo. 2015. A dural lymphatic vascular system that drains brain interstitial fluid and macromolecules. *J. Exp. Med.* 212:991–999. https://doi.org/10.1084/jem.20142290

Atkinson, B.J., S. Kalra, X. Wang, T. Bathala, P. Corn, N.M. Tannir, and E. Jonasch. 2014. Clinical outcomes for patients with metastatic renal cell carcinoma treated with alternative sunitinib schedules. *J. Urol.* 191:611–618. https://doi.org/10.1016/j.juro.2013.08.090

Baldwin, M.E., M.M. Halford, S. Roufail, R.A. Williams, M.L. Hibbs, D. Grail, H. Kubo, S.A. Stacker, and M.G. Achen. 2005. Vascular endothelial growth factor D is dispensable for development of the lymphatic system. *Mol. Cell. Biol.* 25:2441–2449. https://doi.org/10.1128/MCB.25.6.2441-2449.2005

Boulton, M., A. Young, J. Hay, D. Armstrong, M. Flessner, M. Schwartz, and M. Johnston. 1996. Drainage of CSF through lymphatic pathways and arachnoid villi in sheep: measurement of 125I-albumin clearance. *Neuropathol. Appl. Neurobiol.* 22:325–333. https://doi.org/10.1111/j.1365-2990.1996.tb01111.x

Boulton, M., M. Flessner, D. Armstrong, J. Hay, and M. Johnston. 1998. Determination of volumetric cerebrospinal fluid absorption into extracranial lymphatics in sheep. *Am. J. Physiol.* 274:R88–R96.

Bower, N.I., K. Koltowska, C. Pichol-Thievend, I. Virshup, S. Paterson, A.K. Lagendijk, W. Wang, B.W. Lindsey, S.J. Bent, S. Baek, et al. 2017. Mural lymphatic endothelial cells regulate meningeal angiogenesis in the zebrafish. *Nat. Neurosci.* 20:774–783. https://doi.org/10.1038/nn.4558

Brierley, J.B., and E.J. Field. 1948. The connexions of the spinal sub-arachnoid space with the lymphatic system. *J. Anat.* 82:153–166.

Bry, M., R. Kivelä, T. Holopainen, A. Anisimov, T. Tammela, J. Soronen, J. Silvola, A. Saraste, M. Jeltsch, P. Korpisalo, et al. 2010. Vascular endothelial growth factor-B acts as a coronary growth factor in transgenic rats without inducing angiogenesis, vascular leak, or inflammation. *Circulation.* 122:1725–1733. https://doi.org/10.1161/CIRCULATIONAHA.110.957332

Calvo, C.F., R.H. Fontaine, J. Soueid, T. Tammela, T. Makinen, C. Alfaro-Cervello, F. Bonnaud, A. Miguez, L. Benhaim, Y. Xu, et al. 2011. Vascular endothelial growth factor receptor 3 directly regulates murine neurogenesis. *Genes Dev.* 25:831–844. https://doi.org/10.1101/gad.615311

Card, C.M., S.S. Yu, and M.A. Swartz. 2014. Emerging roles of lymphatic endothelium in regulating adaptive immunity. *J. Clin. Invest.* 124:943–952. https://doi.org/10.1172/JCI73316

Cha, Y.R., M. Fujita, M. Butler, S. Isogai, E. Kochhan, A.F. Siekmann, and B.M. Weinstein. 2012. Chemokine signaling directs trunk lymphatic network formation along the preexisting blood vasculature. *Dev. Cell.* 22:824–836. https://doi.org/10.1016/j.devcel.2012.01.011

Choi, I., H.K. Chung, S. Ramu, H.N. Lee, K.E. Kim, S. Lee, J. Yoo, D. Choi, Y.S. Lee, B. Aguilar, and Y.K. Hong. 2011. Visualization of lymphatic vessels by Prox1-promoter directed GFP reporter in a bacterial artificial chromosome-based transgenic mouse. *Blood.* 117:362–365. https://doi.org/10.1182/blood-2010-07-298562

Cserr, H.F., and P.M. Knopf. 1992. Cervical lymphatics, the blood-brain barrier and the immunoreactivity of the brain: a new view. *Immunol. Today.* 13:507–512. https://doi.org/10.1016/0167-5699(92)90027-5

Escobedo, N., and G. Oliver. 2016. Lymphangiogenesis: Origin, Specification, and Cell Fate Determination. *Annu. Rev. Cell Dev. Biol.* 32:677–691. https://doi.org/10.1146/annurev-cellbio-111315-124944

Faivre, S., G. Demetri, W. Sargent, and E. Raymond. 2007. Molecular basis for sunitinib efficacy and future clinical development. *Nat. Rev. Drug Discov.* 6:734–745. https://doi.org/10.1038/nrd2380

Fang, S., H. Nurmi, K. Heinolainen, S. Chen, E. Salminen, P. Saharinen, H.K. Mikkola, and K. Alitalo. 2016. Critical requirement of VEGF-C in transition to fetal erythropoiesis. *Blood.* 128:710–720. https://doi.org/10.1182/blood-2015-12-687970

Field, E.J., and J.B. Brierley. 1948. The lymphatic drainage of the spinal nerve roots in the rabbit. *J. Anat.* 82:198–206.1.

Földi, M., A. Gellért, M. Kozma, M. Poberai, O.T. Zoltán, and E. Csanda. 1966. New contributions to the anatomical connections of the brain and the lymphatic system. *Acta Anat. (Basel).* 64:498–505. https://doi.org/10.1159/000142849

Gaál, E.I., T. Tammela, A. Anisimov, S. Marbacher, P. Honkanen, G. Zarkada, V.M. Leppänen, T. Tatlisumak, J. Hernesniemi, M. Niemelä, and K. Alitalo. 2013. Comparison of vascular growth factors in the murine brain reveals placenta growth factor as prime candidate for CNS revascularization. *Blood.* 122:658–665. https://doi.org/10.1182/blood-2012-07-441527

Gogineni, A., M. Caunt, A. Crow, C.V. Lee, G. Fuh, N. van Bruggen, W.Ye, and R.M. Weimer. 2013. Inhibition of VEGF-C modulates distal lymphatic remodeling and secondary metastasis. *PLoS One.* 8:e68755. https://doi.org/10.1371/journal.pone.0068755

Hägerling, R., C. Pollmann, M. Andreas, C. Schmidt, H. Nurmi, R.H. Adams, K. Alitalo, V. Andresen, S. Schulte-Merker, and F. Kiefer. 2013. A novel multistep mechanism for initial lymphangiogenesis in mouse embryos based on ultramicroscopy. *EMBO J.* 32:629–644. https://doi.org/10.1038/emboj.2012.340

Haiko, P., T. Makinen, S. Keskitalo, J. Taipale, M.J. Karkkainen, M.E. Baldwin, S.A. Stacker, M.G. Achen, and K. Alitalo. 2008. Deletion of vascular endothelial growth factor C (VEGF-C) and VEGF-D is not equivalent to VEGF receptor 3 deletion in mouse embryos. *Mol. Cell. Biol.* 28:4843–4850. https://doi.org/10.1128/MCB.02214-07

He, Y., I. Rajantie, K. Pajusola, M. Jeltsch, T. Holopainen, S. Yla-Herttuala, T. Harding, K. Jooss, T. Takahashi, and K. Alitalo. 2005. Vascular endothelial cell growth factor receptor 3-mediated activation of lymphatic endothelium is crucial for tumor cell entry and spread via lymphatic vessels. *Cancer Res.* 65:4739–4746. https://doi.org/10.1158/0008-5472.CAN-04-4576

Heinolainen, K., S. Karaman, G. D'Amico, T. Tammela, R. Sormunen, L. Eklund, K. Alitalo, and G. Zarkada. 2017. VEGFR3 Modulates Vascular Permeability by Controlling VEGF/VEGFR2 Signaling. *Circ. Res.* 120:1414–1425. https://doi.org/10.1161/CIRCRESAHA.116.310477

His, W. 1865. Ueber ein perivaskulaeres Kanalsystem in den nervoesen Central-Organen und ueber dessen Beziehungen zum *Lymphsystem*. *Z. Wiss. Zool.* 5:127–141.

Honkanen, H.K., V. Izzi, T. Petäistö, T. Holopainen, V. Harjunen, T. Pihlajaniemi, K. Alitalo, and R. Heljasvaara. 2016. Elevated VEGF-D Modulates Tumor Inflammation and Reduces the Growth of Carcinogen-Induced Skin Tumors. *Neoplasia.* 18:436–446. https://doi.org/10.1016/j.neo.2016.05.002

Iliff, J.J., M. Wang, Y. Liao, B.A. Plogg, W. Peng, G.A. Gundersen, H. Benveniste, G.E. Vates, R. Deane, S.A. Goldman, et al. 2012. A paravascular pathway facilitates CSF flow through the brain parenchyma and the clearance of interstitial solutes, including amyloid β. *Sci. Transl. Med.* 4:147ra111. https://doi.org/10.1126/scitranslmed.3003748

Jeltsch, M., S.K. Jha, D. Tvorogov, A. Anisimov, V.M. Leppänen, T. Holopainen, R. Kivelä, S. Ortega, T. Kärpanen, and K. Alitalo. 2014. CCBE1 enhances lymphangiogenesis via A disintegrin and metalloprotease with thrombospondin motifs-3-mediated vascular endothelial growth factor-C activation. *Circulation.* 129:1962–1971. https://doi.org/10.1161/CIRCULATIONAHA.113.002779

Jessen, N.A., A.S. Munk, I. Lundgaard, and M. Nedergaard. 2015. The Glymphatic System: A Beginner's Guide. *Neurochem. Res.* 40:2583–2599. https://doi.org/10.1007/s11064-015-1581-6

Jha, S.K., K. Rauniyar, T. Karpanen, V.M. Leppänen, P. Brouillard, M. Vikkula, K. Alitalo, and M. Jeltsch. 2017. Efficient activation of the lymphangiogenic growth factor VEGF-C requires the C-terminal domain of VEGF-C and the N-terminal domain of CCBE1. *Sci. Rep.* 7:4916. https://doi.org/10.1038/s41598-017-04982-1

Johnson, L.A., S. Banerji, W. Lawrance, U. Gileadi, G. Prota, K.A. Holder, Y.M. Roshorm, T. Hanke, V. Cerundolo, N.W. Gale, and D.G. Jackson. 2017. Dendritic cells enter lymph vessels by hyaluronan-mediated docking to the endothelial receptor LYVE-1. *Nat. Immunol.* 18:762–770. https://doi.org/10.1038/ni.3750

Kamba, T., B.Y. Tam, H. Hashizume, A. Haskell, B. Sennino, M.R. Mancuso, S.M. Norberg, S.M. O'Brien, R.B. Davis, L.C. Gowen, et al. 2006. VEGF-dependent plasticity of fenestrated capillaries in the normal adult microvasculature. *Am. J. Physiol. Heart Circ. Physiol.* 290:H560–H576. https://doi.org/10.1152/ajpheart.00133.2005

Karkkainen, M.J., P. Haiko, K. Sainio, J. Partanen, J. Taipale, T.V. Petrova, M. Jeltsch, D.G. Jackson, M. Talikka, H. Rauvala, et al. 2004. Vascular endothelial growth factor C is required for sprouting of the first lymphatic vessels from embryonic veins. *Nat. Immunol.* 5:74–80. https://doi.org/10.1038/ni1013

Karpanen, T., M. Wirzenius, T. Mäkinen, T. Veikkola, H.J. Haisma, M.G. Achen, S.A. Stacker, B. Pytowski, S. Ylä-Herttuala, and K. Alitalo. 2006. Lymphangiogenic growth factor responsiveness is modulated by postnatal lymphatic vessel maturation. *Am. J. Pathol.* 169:708–718. https://doi.org/10.2353/ajpath.2006.051200

Kazenwadel, J., and N.L. Harvey. 2016. Morphogenesis of the lymphatic vasculature: A focus on new progenitors and cellular mechanisms important for constructing lymphatic vessels. *Dev. Dyn.* 245:209–219. https://doi.org/10.1002/dvdy.24313

Kerjaschki, D. 2014. The lymphatic vasculature revisited. *J. Clin. Invest.* 124:874–877. https://doi.org/10.1172/JCI74854

Kim, H., S.A. Moore, and M.G. Johnston. 2014. Potential for intranasal drug delivery to alter cerebrospinal fluid outflow via the nasal turbinate lymphatics. *Fluids Barriers CNS.* 11:4. https://doi.org/10.1186/2045-8118-11-4

Kim, K.E., H.K. Sung, and G.Y. Koh. 2007. Lymphatic development in mouse small intestine. *Dev. Dyn.* 236:2020–2025. https://doi.org/10.1002/dvdy.21200

Klotz, L., S. Norman, J.M. Vieira, M. Masters, M. Rohling, K.N. Dubé, S. Bollini, F. Matsuzaki, C.A. Carr, and P.R. Riley. 2015. Cardiac lymphatics are heterogeneous in origin and respond to injury. *Nature.* 522:62–67. https://doi.org/10.1038/nature14483

Koch, A.W., T. Mathivet, B. Larrivée, R.K. Tong, J. Kowalski, L. Pibouin-Fragner, K. Bouvrée, S. Stawicki, K. Nicholes, N. Rathore, et al. 2011. Robo4 maintains vessel integrity and inhibits angiogenesis by interacting with UNC5B. *Dev. Cell.* 20:33–46. https://doi.org/10.1016/j.devcel.2010.12.001

Koltowska, K., K.L. Betterman, N.L. Harvey, and B.M. Hogan. 2013. Getting out and about: the emergence and morphogenesis of the vertebrate lymphatic vasculature. *Development.* 140:1857–1870. https://doi.org/10.1242/dev.089565

Kwon, S., C.F. Janssen, F.C. Velasquez, and E.M. Sevick-Muraca. 2017. Fluorescence imaging of lymphatic outflow of cerebrospinal fluid in mice. *J. Immunol. Methods.* 449:37–43. https://doi.org/10.1016/j.jim.2017.06.010

Lindahl, P., B.R. Johansson, P. Levéen, and C. Betsholtz. 1997. Pericyte loss and microaneurysm formation in PDGF-B-deficient mice. *Science.* 277:242–245. https://doi.org/10.1126/science.277.5323.242

Lohrberg, M., and J. Wilting. 2016. The lymphatic vascular system of the mouse head. *Cell Tissue Res.* 366:667–677. https://doi.org/10.1007/s00441-016-2493-8

Louveau, A., I. Smirnov, T.J. Keyes, J.D. Eccles, S.J. Rouhani, J.D. Peske, N.C. Derecki, D. Castle, J.W. Mandell, K.S. Lee, et al. 2015. Structural and functional features of central nervous system lymphatic vessels. *Nature.* 523:337–341. https://doi.org/10.1038/nature14432

Louveau, A., B.A. Plog, S. Antila, K. Alitalo, M. Nedergaard, and J. Kipnis. 2017. Understanding the functions and relationships of the glymphatic system and meningeal lymphatics. *J. Clin. Invest.* 127:3210–3219. https://doi.org/10.1172/JCI90603

Mack, J., W. Squier, and J.T. Eastman. 2009. Anatomy and development of the meninges: implications for subdural collections and CSF circulation. *Pediatr. Radiol.* 39:200–210. https://doi.org/10.1007/s00247-008-1084-6

Mäkinen, T., L. Jussila, T. Veikkola, T. Karpanen, M.I. Kettunen, K.J. Pulkkanen, R. Kauppinen, D.G. Jackson, H. Kubo, S. Nishikawa, et al. 2001. Inhibition of lymphangiogenesis with resulting lymphedema in transgenic mice expressing soluble VEGF receptor-3. *Nat. Med.* 7:199–205. https://doi.org/10.1038/84651

Mancuso, M.R., F. Kuhnert, and C.J. Kuo. 2008. Developmental angiogenesis of the central nervous system. *Lymphat. Res. Biol.* 6:173–180. https://doi.org/10.1089/lrb.2008.1014

Martinez-Corral, I., M.H. Ulvmar, L. Stanczuk, F. Tatin, K. Kizhatil, S.W. John, K. Alitalo, S. Ortega, and T. Makinen. 2015. Nonvenous origin of

dermal lymphatic vasculature. *Circ. Res.* 116:1649–1654. https://doi.org/10.1161/CIRCRESAHA.116.306170

Martinez-Pomares, L. 2012. The mannose receptor. *J. Leukoc. Biol.* 92:1177–1186. https://doi.org/10.1189/jlb.0512231

Nurmi, H., P. Saharinen, G. Zarkada, W. Zheng, M.R. Robciuc, and K. Alitalo. 2015. VEGF-C is required for intestinal lymphatic vessel maintenance and lipid absorption. *EMBO Mol. Med.* 7:1418–1425. https://doi.org/10.15252/emmm.201505731

Oliver, G., and K. Alitalo. 2005. The lymphatic vasculature: recent progress and paradigms. *Annu. Rev. Cell Dev. Biol.* 21:457–483. https://doi.org/10.1146/annurev.cellbio.21.012704.132338

Park, D.Y., J. Lee, I. Park, D. Choi, S. Lee, S. Song, Y. Hwang, K.Y. Hong, Y. Nakaoka, T. Makinen, et al. 2014. Lymphatic regulator PROX1 determines Schlemm's canal integrity and identity. *J. Clin. Invest.* 124:3960–3974. https://doi.org/10.1172/JCI75392

Paxinos, G., and K.B.J. Franklin. 2001. The Mouse Brain in Stereotaxic Coordinates. Academic Press Inc., Orlando, FL. 264 pp.

Petrova, T.V., A. Nykänen, C. Norrmén, K.I. Ivanov, L.C. Andersson, C. Haglund, P. Puolakkainen, F. Wempe, H. von Melchner, G. Gradwohl, et al. 2008. Transcription factor PROX1 induces colon cancer progression by promoting the transition from benign to highly dysplastic phenotype. *Cancer Cell.* 13:407–419. https://doi.org/10.1016/j.ccr.2008.02.020

Pitulescu, M.E., I. Schmidt, R. Benedito, and R.H. Adams. 2010. Inducible gene targeting in the neonatal vasculature and analysis of retinal angiogenesis in mice. *Nat. Protoc.* 5:1518–1534. https://doi.org/10.1038/nprot.2010.113

Pollay, M. 2010. The function and structure of the cerebrospinal fluid outflow system. *Cerebrospinal Fluid Res.* 7:9. https://doi.org/10.1186/1743-8454-7-9

Ruberte, J., A. Carretero, and M. Navarro. 2017. Morphological Mouse Phenotyping: Anatomy, Histology and Imaging. Elsevier, Boston. 585 pp.

Schoppmann, S.F., R. Horvat, and P. Birner. 2002. Lymphatic vessels and lymphangiogenesis in female cancer: mechanisms, clinical impact and possible implications for anti-lymphangiogenic therapies. *Oncol. Rep.* 9:455–460.

Schwalbe, G. 1869. Die Arachnoidalraum, ein Lymphraum und sein Zusammenhang mit den Perichorioidalraum. *Zentralbl Med Wiss.* 7:465–467.

Secker, G.A., and N.L. Harvey. 2015. VEGFR signaling during lymphatic vascular development: From progenitor cells to functional vessels. *Dev. Dyn.* 244:323–331. https://doi.org/10.1002/dvdy.24227

Stanczuk, L., I. Martinez-Corral, M.H. Ulvmar, Y. Zhang, B. Laviña, M. Fruttiger, R.H. Adams, D. Saur, C. Betsholtz, S. Ortega, et al. 2015. cKit Lineage Hemogenic Endothelium-Derived Cells Contribute to Mesenteric Lymphatic Vessels. *Cell Rep.* https://doi.org/10.1016/j.celrep.2015.02.026

Sun, B.L., L.H. Wang, T. Yang, J.Y. Sun, L.L. Mao, M.F. Yang, H. Yuan, R.A. Colvin, and X.Y. Yang. 2017. Lymphatic drainage system of the brain: A novel target for intervention of neurological diseases. *Prog. Neurobiol.* https://doi.org/10.1016/j.pneurobio.2017.08.007

Tammela, T., A. Saaristo, T. Holopainen, J. Lyytikkä, A. Kotronen, M. Pitkonen, U. Abo-Ramadan, S. Ylä-Herttuala, T.V. Petrova, and K. Alitalo. 2007. Therapeutic differentiation and maturation of lymphatic vessels after lymph node dissection and transplantation. *Nat. Med.* 13:1458–1466. https://doi.org/10.1038/nm1689

Tarasoff-Conway, J.M., R.O. Carare, R.S. Osorio, L. Glodzik, T. Butler, E. Fieremans, L. Axel, H. Rusinek, C. Nicholson, B.V. Zlokovic, et al. 2015. Clearance systems in the brain-implications for Alzheimer disease. *Nat. Rev. Neurol.* 11:457–470. https://doi.org/10.1038/nrneurol.2015.119

Vaahtomeri, K., S. Karaman, T. Mäkinen, and K. Alitalo. 2017. Lymphangiogenesis guidance by paracrine and pericellular factors. *Genes Dev.* 31:1615–1634. https://doi.org/10.1101/gad.303776.117

van Lessen, M., S. Shibata-Germanos, A. van Impel, T.A. Hawkins, J. Rihel, and S. Schulte-Merker. 2017. Intracellular uptake of macromolecules by brain lymphatic endothelial cells during zebrafish embryonic development. *eLife.* 6:e25932. https://doi.org/10.7554/eLife.25932

Venero Galanternik, M., D. Castranova, A.V. Gore, N.H. Blewett, H.M. Jung, A.N. Stratman, M.R. Kirby, J. Iben, M.F. Miller, K. Kawakami, et al. 2017. A novel perivascular cell population in the zebrafish brain. *eLife.* 6:e24369.

Ventura, A., D.G. Kirsch, M.E. McLaughlin, D.A. Tuveson, J. Grimm, L. Lintault, J. Newman, E.E. Reczek, R. Weissleder, and T. Jacks. 2007. Restoration of p53 function leads to tumour regression in vivo. *Nature.* 445:661–665. https://doi.org/10.1038/nature05541

Walter, B.A., V.A. Valera, S. Takahashi, and T. Ushiki. 2006. The olfactory route for cerebrospinal fluid drainage into the peripheral lymphatic system. *Neuropathol. Appl. Neurobiol.* 32:388–396. https://doi.org/10.1111/j.1365-2990.2006.00737.x

Welti, J., S. Loges, S. Dimmeler, and P. Carmeliet. 2013. Recent molecular discoveries in angiogenesis and antiangiogenic therapies in cancer. *J. Clin. Invest.* 123:3190–3200. https://doi.org/10.1172/JCI70212

Wigle, J.T., and G. Oliver. 1999. Prox1 function is required for the development of the murine lymphatic system. *Cell.* 98:769–778. https://doi.org/10.1016/S0092-8674(00)81511-1

Zakharov, A., C. Papaiconomou, J. Djenic, R. Midha, and M. Johnston. 2003. Lymphatic cerebrospinal fluid absorption pathways in neonatal sheep revealed by subarachnoid injection of Microfil. *Neuropathol. Appl. Neurobiol.* 29:563–573. https://doi.org/10.1046/j.0305-1846.2003.00508.x

Zudaire, E., L. Gambardella, C. Kurcz, and S. Vermeren. 2011. A computational tool for quantitative analysis of vascular networks. *PLoS One.* 6:e27385. https://doi.org/10.1371/journal.pone.0027385